Schweizerische Eidgenossenschaft
Confédération suisse
Confederazione Svizzera
Confederaziun svizra

Eidgenössisches Departement für
Umwelt, Verkehr, Energie und Kommunikation UVEK

Bundesamt für Energie BFE
Sektion Energieforschung und Cleantech

Schlussbericht vom 01.12.2020

Verbesserte Windkraftanlage mit innovativem Gondel-Entwicklung

Improved Wind Turbine Performance Using Innovative Nacelle Design

Quelle: Hitachi Ltd.

Datum: 01.12.2020

Ort: Bern

Subventionsgeberin:
Bundesamt für Energie BFE
Sektion Energieforschung und Cleantech
CH-3003 Bern
www.bfe.admin.ch

Ko-Finanzierung:
Agentur XY
Strasse, CH-PLZ Ort
www.agentur-xy.ch

Subventionsempfänger/innen:
Institution X
Strasse, CH-PLZ Ort
www.institution-x.ch

Institution Y
Strasse, CH-PLZ Ort
www.institution-y.ch

Autor/in:
Ndaona Chokani, Laboratory for Energy Conversion, ETH Zürich, chokanin@ethz.ch
Reza Abhari, Laboratory for Energy Conversion, ETH Zürich, abhari@ethz.ch

BFE-Projektbegleitung:
Katja Maus, katja.maus@bfe.admin.ch
Lionel Perret, lionel.perret@Planair.ch

BFE-Vertragsnummer: SI/501107-01

Für den Inhalt und die Schlussfolgerungen sind ausschliesslich die Autoren dieses Berichts verantwortlich.

Zusammenfassung

Eine neuartige vergleichende Studie über die Wirksamkeit einer optimierten Gondel unter Verwendung von Klappen zur Verringerung der Ermüdungsbelastung und zur Verbesserung der Leistung von Windkraftanlagen wird experimentell durchgeführt. Die Experimente werden an einem maßstabgetreuen Modell einer kommerziellen 2MW-Windturbine mit einer Rotorneigung von 8° und einem Konuswinkel von 5° durchgeführt; das Modell kann sowohl in Auf- als auch in Abwind-konfigurationen getestet werden. Das Modell ist mit an der Turmfußwurzel montierten Dehnungsmessstreifen und einem speziell angefertigten Inline-Drehmomentmesser instrumentiert, von dem aus die Zeitverläufe von Schub, Biegemoment, Torsionsmoment und Drehmoment gemessen werden. Die verschiedenen Klappenwinkel werden zur Verringerung der Ermüdungsbelastung und zur Verbesserung der Turbinenleistung eingesetzt. Eine umfassende Analyse der gemessenen Lastschwankungen im gesamten Phasengang, die auf den nieder- und hochfrequenten Schwankungen des gemessenen Rotorschubs und -drehmoments basiert, wird verwendet, um den Einfluss der Klappen auf die kumulativen Blattschäden und die Ermüdungslebensdauer sowohl für Auf- als auch für Abwind-konfigurationen zu bewerten. Die detaillierten experimentellen Ergebnisse werden durch theoretische Erläuterungen ergänzt, die dazu dienen, Einblicke in die experimentellen Ergebnisse sowohl für Auf- als auch für Abwind-konfigurationen zu geben. Es hat sich gezeigt, dass Klappen, die in der Vorwind-konfiguration vor dem Rotor installiert sind, die Strömung im Vergleich zur Aufwind-konfiguration effektiver in Richtung der äußeren Spannweiten drücken; dies stimmt mit den Experimenten überein. Aus praktischer Sicht wird eine Strategie des Einsatzes von Klappen zur Minderung von kumulativen Blattschäden sowie zur Verbesserung der Turbinenleistung und der Gierstabilität sowohl bei Auf- als auch bei Abwind-konfigurationen empfohlen.

Summary

A novel comparative study of the effectiveness of optimised nacelle using flaps to alleviate fatigue loads and to improve performance of wind turbines is experimentally conducted. The experiments are accomplished on a scale model of a commercial 2MW wind turbine that has a rotor tilt of 8°, and a cone angle of 5°; the model can be tested in both upwind and downwind configurations. The model is instrumented with tower root-mounted strain gauges and a custom-built in-line torque meter from which time histories of thrust, bending moment, twisting moment, and torque are measured. The different flaps angles are applied to alleviate fatigue loads and to improve turbine power. An extensive full phase domain analysis of the measured load variations, based on the low and high-frequency fluctuations of measured rotor thrust and torque, is used to assess the impact of the flaps on the blade cumulative damage and the fatigue lifetime for both upwind and downwind configurations. The detailed experimental results are complemented with theoretical explanations that are used to provide insights into the experimental findings for both upwind and downwind configurations. Flaps installed upstream of the rotor in the downwind configuration are shown to be more effective in pushing the flow towards outer spans compared to the upwind configuration; this is in agreement with the experiments. From a practical standpoint, a strategy of using flaps to mitigate blade cumulative damage, as well as to improve turbine power and yaw stability for both upwind and downwind configurations, is recommended.

Take-Home Messages

- As a passive approach, using flaps not only alleviates unsteady loads and therefore extends the fatigue lifetime of blades but also improves turbine power and yaw stability.
- Flaps installed upstream of the rotor in the downwind configuration are shown to be more effective in pushing the flow towards outer spans compared to the upwind configuration.
- Using flaps in downwind configuration compensates for the adverse effect of wind turbine yaw misalignment on the wind turbine performance and unsteady loads. Furthermore, using flaps decreases the cut-in speed and therefore increases the turbine annual energy yield by increasing wind turbine power generation for downwind configuration.
- Theoretical explanations indicate that in the case of upwind configuration, increasing downstream velocity (slowing down upstream velocity) leads to a marginally decrease in turbine power (turbine Euler equation) and consequently may marginally increase the torque amplitude ratio. However, lower wind speeds seen by inner spans lead to mitigate thrust load generated by inner spans. In the case of downwind configuration, increasing upstream velocity leads to improve turbine power based on the turbine Euler equation, and pushing flow to outer spans with higher lift/drag ratios leads to mitigate unsteady loads (thrust and torque) generated by inner spans.

Table of Contents

List of Abbreviations

P	turbine power
V	inflow velocity
T	turbine shaft torque
M	twist moment of tower
λ	tip speed ratio
α	flap angle
C_P	coefficient of power
C_T	coefficient of thrust
C_M	coefficient of moment
C_{M0}	coefficient of moment without yaw
C_{P00}	coefficient of the power without yaw and no flap
C_{T00}	coefficient of the thrust without yaw and no flap
C_{M00}	coefficient of the moment without yaw and no flap
σ_a	amplitude of major stress
σ_b	amplitude of minor stress
σ_m	mean of major stress
σ_r	range of stress
σ_{max}	maximum stress
σ_{min}	minimum stress
D_t	total cumulative damage
D_i	cumulative damage fraction
n_i	number of loading cycles at the stress level of σ_i
N_{Ri}	number of cycles to failure at σ_i
k	number of stress levels
φ	incidence angle
L	lift force
D	drag force
F_N	axial force
F_T	tangential force
V_{rel}	relative velocity
F_R	result force
C_L	lift coefficient
C_D	drag coefficient

1 Introduction

1.1 Initial Situation and Background

In May 2017, Swiss voters endorsed the Federal government's strategy of further exploiting hydropower and other renewable resources (such as wind farms and photovoltaic installations), as well as increasing energy efficiency. No new nuclear power plants will be built in Switzerland, and the existing nuclear power plants are to be decommissioned at the end of their technically safe operating life. These measures, which are part of Switzerland's Energy Strategy 2050 (ES2050) [1], were an outcome of the Swiss parliament's decision to initiate the phase-out of nuclear power by 2050 in reaction to the Fukushima nuclear accident. Solar and wind now account for less than 5% of Switzerland's energy output, compared with 60% for hydropower and 35% for nuclear [2]. In the framework of ES2050, non-hydro renewable power is planned to have a fourfold increase from 2,831GWh now to at least 11,400GWh by 2035 [3]. Thus, wind-generated electricity shall comprise a significant portion of non-hydro renewables in Switzerland's future energy mix. In addition to energy efficiency and renewable energies, ES2050 emphasises two more guiding principles: firstly, securing the sourcing of foreign energy, and secondly, planning the replacement and construction of alternative electricity-producing power plants. The sourced foreign energy shall largely comprise of solar and wind power, as the EU has established a target of 45% renewable electricity by 2030 [4]. Thus both Swiss and European wind-generated electricity shall be an important component of the future energy mix. Therefore, advances in wind turbine technology will have a positive impact on accomplishing the goals of ES2050.

1.2 Project Motivation

To maximise the performance of wind turbines, a number of different approaches have been widely examined. The most common approach is to optimise the rotor design, in particular, the aerostructural design of rotor blades. Another approach is to apply retrofits to the rotor blades, for example, vortex generators. Vortex generators have been demonstrated to increase a turbine's annual energy yield by 1.5-3%. On the other hand, for the purpose of improving the performance of wind turbines, the design of the nacelle shape has received little or no attention. However, computational simulations at ETH show that the nacelle can result in significant increases in the annual energy yield of wind turbines [5]. One reason that the design of the nacelle shape has not been considered as a means of improving the performance of wind turbines is that the size of turbines has increased in recent years, as wind-generated electricity has become more cost-competitive. On modern multi-megawatt turbines, the components contained within the nacelle are heavy (that is hundreds of tons in weight); therefore, in many cases, transportation costs of nacelles exceed the nacelle's manufacturing costs. Thus, the primary driver in the design of nacelles has been to design the nacelles to be compact and lightweight, such that the nacelles can be transported on roads and meet the required clearances under bridges and through tunnels. In a computational fluid dynamic (CFD) study that compares the performance of downwind and upwind configurations of wind turbines, the present authors observed that the nacelle on a downwind wind turbine acts both as a blockage to the incoming flow and as an accelerator of the flow into the rotor [5]. This observation indicated that an optimisation of the nacelle shape on downwind turbines can yield substantial increases in the annual energy yield, with increases substantially exceeding even the increases obtained from the use of vortex generators.

1.3 Project Goals

The goals of this project are: (i) to experimentally and computationally demonstrate that optimised nacelle shapes on downwind turbines can yield substantial increases in annual energy yield; (ii) to develop engineering models to optimise the nacelle shape; and (iii) to promote to domestic and international industry innovative designs of nacelle housings as a business case that can advance their positions in the global marketplace of the wind industry. These goals are relevant increasing the contribution of wind-generated electricity production in Switzerland's future energy mix, which is in accordance with Switzerland's "Energy Strategy 2050." To address the goals of this project, the effect of the nacelle on turbine performance is investigated. Nacelle designs are then tested in an experimental setup in WEST Facility.

The final results of the comparative experimental study of the effectiveness of optimised nacelle shape using flaps on fatigue loads alleviation and performance improvement of multi-megawatt wind turbines are presented in this report. Inner spans mainly function as stiffeners and stress support rather than generating power, while turbine power is mainly generated over the outer spans. Therefore, it is always a challenge to reduce the effect of inner spans in generating wind turbines unsteady loads. Thus, the idea is to optimise wind turbine nacelles using flaps to push the flow towards outer spans which leads to improved turbine performance, as well as mitigates unsteady loads, therefore, extending the fatigue life of wind turbine's components. Moreover, the cut-in speed of wind turbines (especially in downwind configuration) can be decreased and the turbine annual energy yield can be increased. It is shown that using flaps to optimise the nacelle shape not only mitigates unsteady loads and therefore extends the fatigue lifetime of blades but also improves turbine power and yaw stability. The detailed experimental results are complemented with theoretical explanations that are used to provide insights into the experimental findings for both upwind and downwind configurations. The theoretical analysis shows that flaps installed upstream of the rotor in the downwind configuration are more effective in pushing the flow towards outer spans in comparison to the upwind con-figuration; this is in agreement with experiments. A strategy of using flaps to mitigate blade cumulative damage, as well as to improve turbine power and yaw stability for both upwind and downwind configurations, is recommended.

2 Operation of Modern Multi-Megawatt Wind Turbines

The operation of wind turbines can be well described from the wind turbine's power curve (Figure 1). In 'Region 1,' at wind speeds below the cut-in wind speed, the wind turbine does not operate, and no power is generated. In 'Region 2,' where the wind speeds are between the cut-in and rated wind speeds, the wind turbine is operated. As the available wind power increases in proportion to the cube of the wind speed, there is a commensurate increase in the generated power of the wind turbine with an increase in wind speed. At the rated wind speed, the generated power equals the rated power of the generator, and thus in 'Region 3,' where the wind speeds are between the rated wind speed and the cut-out wind speed, the generated power is constant. Above the cut-out wind speed, the wind turbine is shutdown, in order to preserve the structural integrity of the wind turbine, and therefore no power is generated. In 'Region 2' of the turbine's operation it is desirable to operate the wind turbine at maximum aerodynamic efficiency, as the wind speed is relatively low in this region, opening the installed flaps on the nacelle is more effective than in 'Region 3' where the wind speed is higher and the flaps lead to more adverse effects of increased drag and unsteadiness.

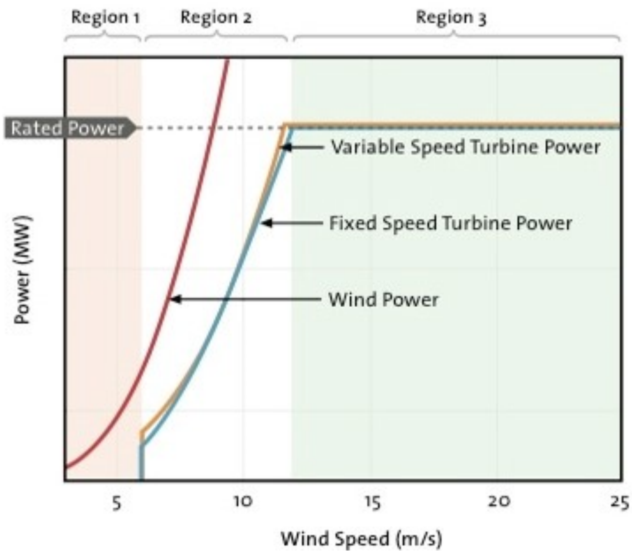

Figure 1. Operating regions of modern wind turbines.

3 Methodology

3.1 ETH Zurich Wind Turbine Test Facility

The experimental work of this project was carried out in ETH's Wind Turbine Test Facility (WEST Facility), Figure 2. The WEST Facility is an open section flow channel (40m long, 1m wide, and 1m deep). The carriage traverses the channel at a constant velocity and moves the model through the water. An active turbulence generator injects water as counter-flowing jets perpendicular to carriage motion through holes of streamlined aerofoils to generate a freestream turbulence intensity of 8%. The shaft torque, turbine thrust, tower twisting, and bending moments are measured at a sampling rate of 10kHz [6].

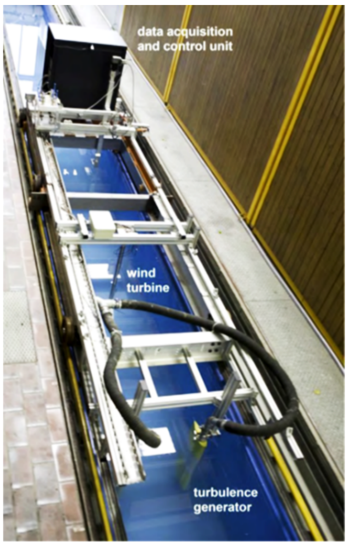

Figure 2: Bird's eye view of the ETH WEST Facility.

3.2 2MW Wind Turbine Model

The experimental study of optimised nacelle shape using flaps is conducted using a 1:160 scale model of the Hitachi HTW2.0-80 (Figure 3) wind turbine in the wind turbine test facility (WEST Facility) at ETH Zurich. The specifications of the full-scale turbine are provided in Table 1. The model has a rotor diameter of 0.5m. The rotor tilt and blade cone angles are 8° and 5°, respectively. The carriage velocity and turbine speed control the tip speed ratio (λ) of the model which is the same as that of the full-scale turbine. At the design tip speed ratio (λ_{design}), the turbine rotational speed (N) is 488 rpm. The model Reynolds number based on the blade chord length at 75% span is approximately 1.1×10^5 [6].

All linear dimensions of the model are scaled-down similarly based on geometrical scaling laws [7]. However, in order to accommodate the required instrumentation and the functionality of an adjustable rotor cone, the geometric scaling of the model's hub is 86% larger than what it would be for a 1:160 scale-model. It is worth noting that the nacelle is also over-scaled compared to a 1:160-scale model mainly due to the size of the drive motor. The model's tower is also over-scaled to provide a sufficient safety factor against bending fracture and to provide sufficient space inside the tower for cable routing [6]. Figure 4 shows the 2MW wind turbine model.

Figure 3. Hitachi HTW2.0-80 wind turbine installed at Kamisu wind farm; courtesy of Wind Power Ltd.

Table 1. Specifications of Hitachi HTW2.0-80 downwind turbine.

Rated power	2MW
Rotor diameter	80m
Blade length	39m
Hub height	65m and 78m
Tilt angle	8º
Cone angle	5º
Blade number	3
Wind class	IIA

The model is of a modular design. The model's parameter range is compared to the full-scale in Table 2. The rotor orientation is easily switched from downwind to upwind configuration by turning the nacelle and the blades 180º around the tower and blade pitch axis, respectively. More details about the design of the 2MW wind turbine model can be found in [6].

Figure 4. Photograph of Hitachi HTW2.0-80 wind turbine model at the ETH WEST Facility, Zurich.

Table 2. 2MW model parameters and ranges.

	Full scale	Model
Rotor configuration	downwind	downwind, upwind
Rotor rotation	counter-clockwise (looking upstream)	counter-clockwise (looking upstream)
Rotor diameter	80m	0.5m
Tilt angle	8º	8º
Cone angle	5º	5º
Rotor yaw	variable	-35º to +35º
TSR	variable	fixed to design value

3.3 Optimised Nacelle Shape Using Flaps

Generally, multi-megawatt wind turbine blades can be sub-divided into the inner and outer spans. The inner spans mainly function as stiffeners and stress support rather than generating power, while the turbine power is mainly generated over the outer spans. Figure 5 shows the inner and outer blade spans for the 2MW wind turbine model. It should be noted that the inner spans blade sections:

- Experience low relative velocities and high incidence angles (relative to outer spans).
- Have low lift/drag ratio (even < 1).
- Generally, do not contribute to generating power, but generate thrust.

Therefore, it is always a challenge to reduce the effect of inner spans in generating unsteady loads.

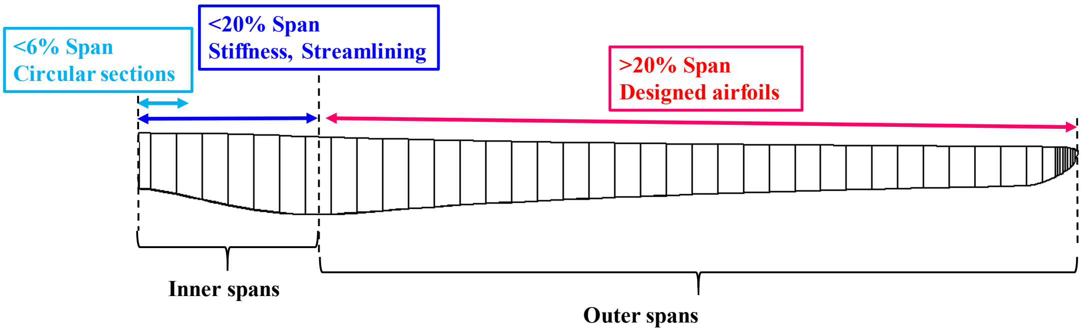

Figure 5. Schematic of the inner and outer blade spans for the 2MW wind turbine model.

As multi-megawatt wind turbines mostly operate in Region II (low and moderate wind speeds, Figure 6), in which the Tip Speed Ratio (TSR) is high and the efficiency is maximum, improving wind turbine performance as well as reducing unsteady loads may have positive impacts on the reliable operation of turbines (and therefore, on operation and maintenance costs), on the energy that is produced (therefore, on revenues), and on the lifetime of the turbines (therefore, on the return of investment). Thus, the idea is to optimise wind turbine nacelles using flaps to push the flow towards outer spans which leads to improved wind turbine performance, as well as mitigates unsteady loads, therefore, extending the fatigue life of wind turbine's components. Moreover, the flaps can decrease the cut-in speed of wind turbines, thus, increasing the turbine annual energy yield.

The aerodynamic characteristics of the Hitachi 2MW wind turbine blade are shown in Figure 7. It is evident that by blocking the inner spans (<20% span), the flow is pushed towards outer spans (>20% span) which have a much higher lift/drag coefficient. On the other hand, flaps block the inner spans which do not contribute to generating power, but generate thrust and unsteady loads.

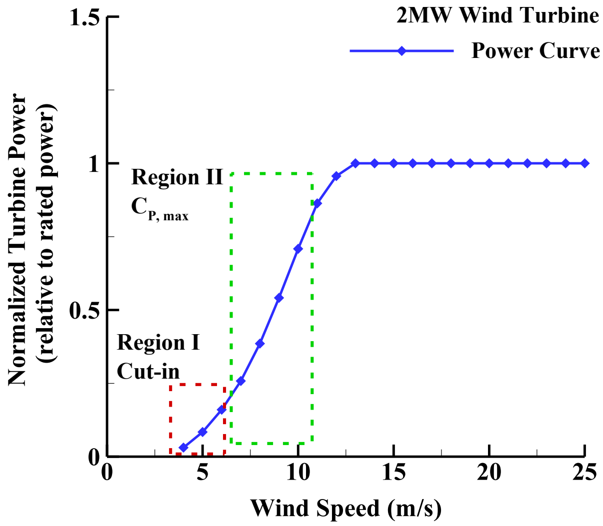

Figure 6. Power curve of the 2MW Hitachi wind turbine.

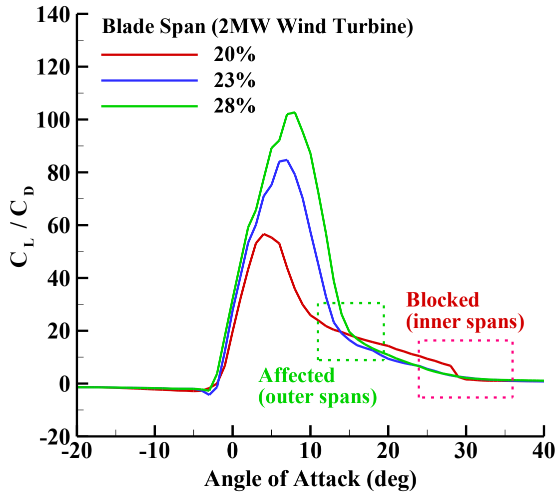

Figure 7. Aerodynamic characteristics of the 2MW Hitachi wind turbine blade.

The flaps can be installed across the whole length of full-scale turbine nacelle in both upwind and downwind configurations. There is also the possibility of installing the flaps on the full-scale nacelle with joint supports and hydraulic systems in order to close the flaps at higher wind speeds or to adjust the flap angle (span blockage) based on the operating conditions. Figure 8 and Figure 9 show the conceptual design of the flaps' installation on the full-scale and sub-scales wind turbines, respectively. It is worth noting that due to the enlarged nacelle of the wind turbine model at the WEST facility, wooden flaps are glued on the nacelle fairing in order to have the same span blockage as on the full-scale for both upwind and downwind configurations as shown in Figure 10.

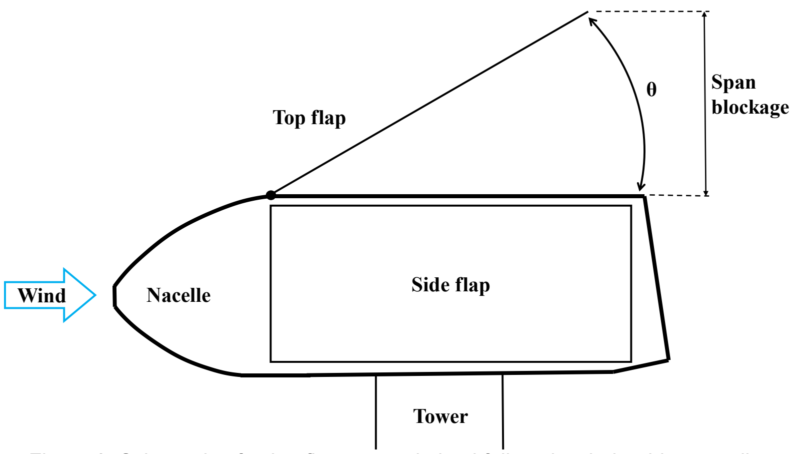

Figure 8. Schematic of using flaps on optimised full-scale wind turbine nacelle.

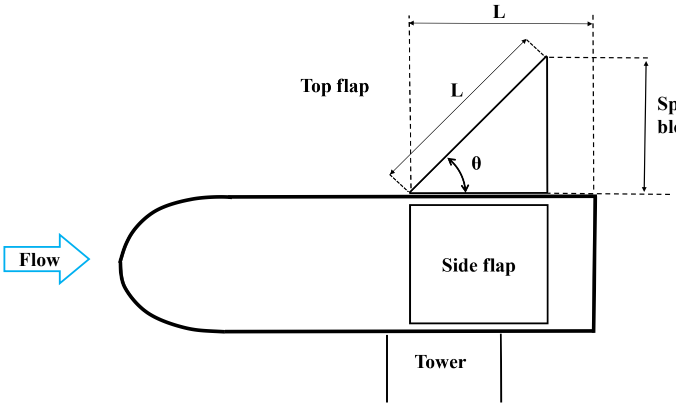

Figure 9. Schematic of using flaps on optimised sub-scale wind turbine nacelle.

Upwind Downwind

Figure 10. Photograph of installed flaps on optimised sub-scale wind turbine nacelle in upwind (left) and downwind (right) configuration.

In order to experimentally investigate the effectiveness of the flaps with different angles on the turbine performance, different flap angles of 30º, 45º, and 60º which correspond to span blockages of 12%, 17%, and 20%, respectively as shown in Figure 11, have been considered. Table 3 summarises the test matrix which is experimentally examined.

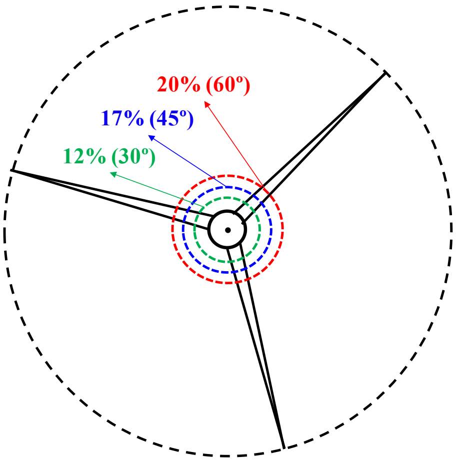

Figure 11. Different span blockages and corresponding flap angles.

Table 3. Test matrix of experimental study.

Parameter	Range
Rotor configuration	Upwind/Downwind
Yaw angle	0°, ±8°, ±16°
Tip speed ratio	λ_{design}
Duration of each measurement	8sec
Flap angles	0°, 30°, 45°, 60°

3.4 Engineering Model

The geometrical arrangement of the flaps is represented within the BEM algorithm. The surface mesh of the nacelle is adapted accordingly. The flaps are not modeled as flat plates. Potential flow is assumed in the 3D panel method. In potential flow, separation around inclined flat plates is not considered. The zone behind flaps is modeled as solid and the wind velocity in this zone is set to zero. The surface mesh of the nacelle with the flap geometry is shown in Figure 12.

Performance changes of the wind turbine by different geometrical arrangements of the flaps are assessed. Generic geometrical arrangements are possible. Three important parameters are specified preliminary to focus the detailed analysis: ‘Span Blockage’, ‘Distance to Rotor’, and ‘Inclination Angle’. The quantification of their impact is focused on the power coefficient at rated wind speed for the preliminary analysis.

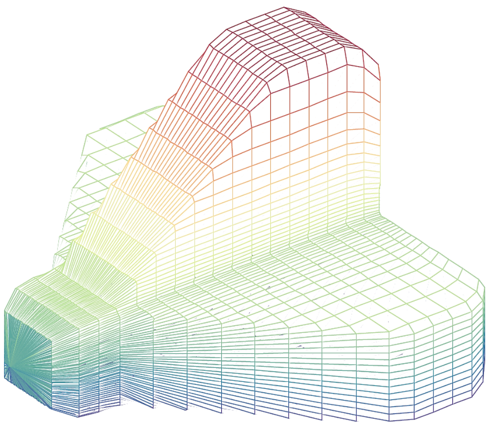

Figure 12: Nacelle surface meshes with flap geometry.

To isolate the effect of the span blockage, the inclination angle is set to 45°. Figure 13 shows the effect of span blockage on the power coefficient. At 30% span blockage, the power coefficient C_P is increased by 1.45%.

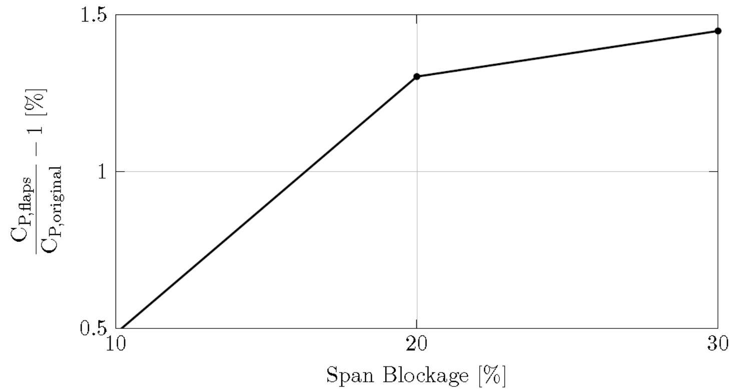

Figure 13: Effect of span blockage on C_P at rated wind speed. The flap inclination angle is 45°.

The effect of the horizontal distance of the flap joint to the rotor is assessed. The schematic drawing of the respective flap configuration is shown in Figure 14. The span blockage is set to 20% and the inclination angle to 45°. The flaps are fixed on the nacelle surface. The horizontal position of the flaps is therefore bounded to the nacelle length. The maximal distance measures 21% and the minimum 11% of the blade radius. Figure 15 shows that the maximum power coefficient is observed at the maximum distance. Moving flaps to the minimum distance decrease the power coefficient by 0.15%.

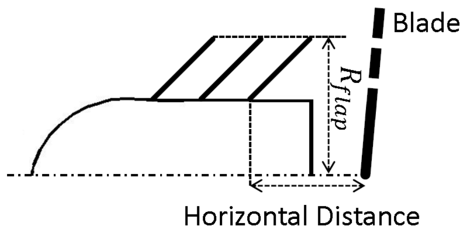

Figure 14: Schematic drawing of the horizontal distance.

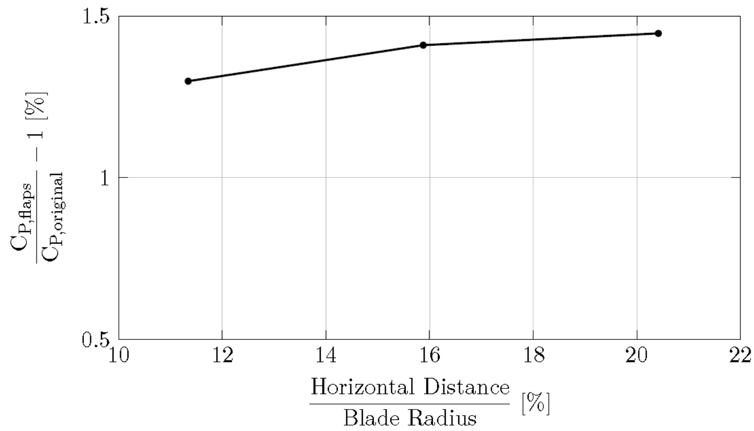

Figure 15: Effect of horizontal distance on C_P at rated wind speed. The flap inclination angle and the span blockage are 45° and 20%, respectively.

The effect of the inclination angle of the flaps is assessed. The flap tip is fixed at the nacelle end as shown in Figure 16. The span blockage is 20%. Increasing the inclination angle decreases the power coefficient as shown in Figure 17. An inclination of 80° decreases the power coefficient by 0.35%.

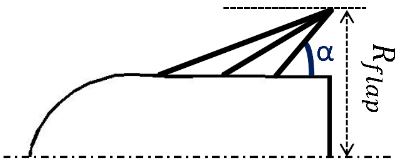

Figure 16: Schematic drawing of flap inclination angle.

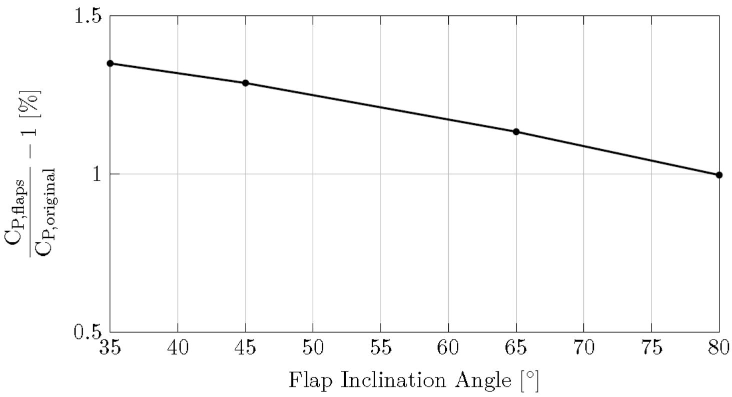

Figure 17: Effect of flap inclination angle on C_P at rated wind speed. The span blockage is 20%.

It can be summarised that the power coefficient can be raised by increasing the span blockage, decreasing the inclination angle, and increasing the distance to the rotor. The effect of the span blockage is dominating. The flap configuration considered in more detail combines the preliminary analysis. To maximize the distance to the rotor, the flap joint is fixed at the rear part of the nacelle. Additionally, the maximal flap length is obtained by covering the whole flat part of the nacelle, as shown in Figure 18. By increasing the flap angle, the span blockage can be increased. For better readability, different flap geometries are quantified by the flap angle. The respective correlation is shown in Table 4.

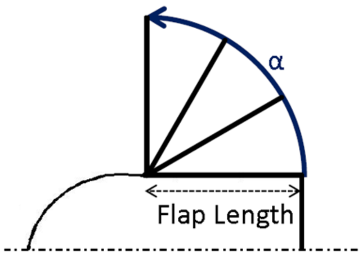

Figure 18: Schematic drawing of considered flap configuration.

Table 4. Correlation of flap angle to span blockage.

Flap angle	Span blockage
15°	6%
30°	12%
40°	15%
45°	17%
50°	18%
60°	20%
75°	22%
85°	23%

3.4.1 Grid Study and Validation

The panel method requires meshing of the nacelle geometry as explained above. The spacing of the surface mesh is expected to influence the BEM simulation results. Therefore, a grid study is conducted. In Figure 19 the errors introduced by the grid spacing are shown. Above 1000 grid points the errors decrease. With 3600 Grid points, the error introduced by the grid spacing is 0.13% and 0.16% in C_P and C_T, respectively. The simulations are conducted with 3600 grid points because the errors are considered to be acceptable. It is worth noting that the continuity equation is fulfilled. The mass flow error is 0.8‰.

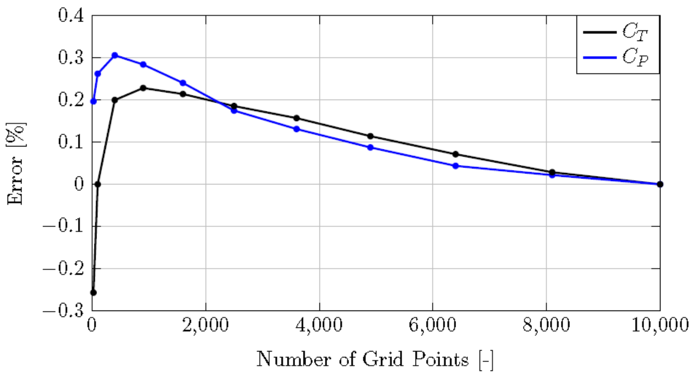

Figure 19: Error in C_P and C_T introduced by the grid spacing.

To validate the BEM-3D panel method combination the results are compared to data available from Kress [6]. In Figure 20 the confrontation with the CFD results is shown. The BEM code simulates the same power coefficient C_P as CFD. The thrust coefficient C_T, on the other hand, is overrated by 4%. The simulation results with the downscaled geometry are illustrated in Figure 21. The measured power coefficient C_P is underrated by 3%. The thrust coefficient C_T is simulated 2% higher.

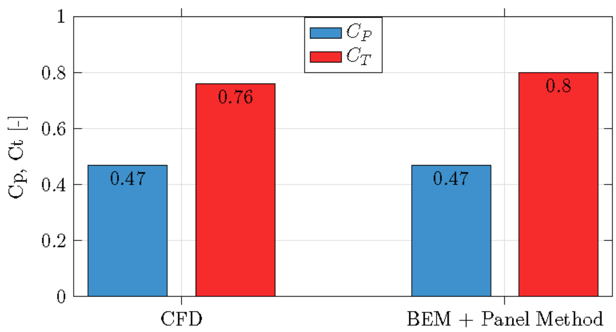

Figure 20: Comparison of BEM simulation results with CFD.

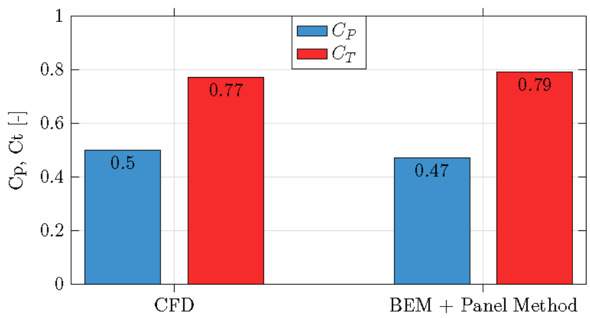

Figure 21: Comparison of BEM simulation results with experiments.

3.5 Blade Cumulative Fatigue Damage

A multi-segmented S-N curve is typically required to characterize the low and high cycle fatigue behavior of composites. As design lifetime is relatively long for wind turbine applications, the low cycle region of the curve is typically not important [8] and the blade's material characteristics in the high cycle fatigue regime are considered for wind turbine applications [9]. Generally, blades are expected to experience 10^8 to 10^9 fatigue cycles over a 20 to 30 year lifetime [10]. The most widely used method of estimating the fatigue life of a component is Miner's rule. Miner's rule can be used to assess the fatigue damage accumulation under variable loading conditions [11,12] as follows:

$$D_t = \sum_{i=1}^{k} D_i = \sum_{i=1}^{k} \frac{n_i}{N_{Ri}} \quad (1)$$

where D_t is the total cumulative damage, D_i is the cumulative damage fraction, n_i is the number of loading cycles at the stress level of σ_i, N_{Ri} is the number of cycles to failure at σ_i, and k is the number of stress levels.

As each measurement is conducted at a specific operating condition (λ_{design} and n_i), in order to assess the effectiveness of flaps on the blade cumulative damage fraction, the number of cycles to failure (N_{Ri}) is calculated with and without flaps using the Double Goodman technique [13,14]. The Double Goodman technique is applied to the two subdivisions of azimuthal variations which are: a) major cycles and b) major and minor cycles, as shown in Figure 22. The azimuthal variation of the measured loads (amplitude ratio or σ_a/σ_m) is considered as the major cycle (σ_m, σ_a, and σ_r) and unsteadiness of the measured loads at the rotor frequency (1P), the blade passing frequency (3P) as well as high-frequency vortex-shedding of the rotor and other harmonics are considered as the minor cycle (σ_b) in the Double Goodman method. The variance is determined from the integral of the power spectral density of the measured unsteady loads. In the case of '1P', '3P', 'Rotor Vortex' variances the bandwidths of integration are ±10% of the rotational speed frequency, blade passing frequency, and vortex-shedding frequency (20P), respectively and the 'Others' variance is determined from the integral outside these bandwidths.

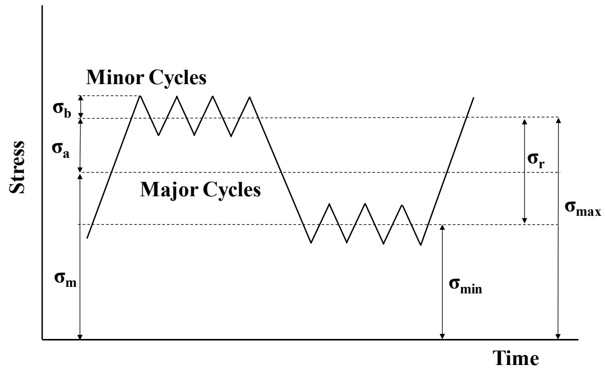

Figure 22. Time variation of unsteady stress.

4 Results and Discussion

4.1 Simulation Results (Downwind configuration)

The effect of flaps on the torque per blade is discussed first for clarification. The wind turbine power corresponds to the aerodynamic torque exerted on the blades. The flaps change the velocity field at the rotor plane compared with the velocity field around the original nacelle geometry. Because the blades are passing a different velocity field, the aerodynamic torque is modified. The analysis of modified torque per blade is exemplified on the 60° flaps. The simulation results with the original nacelle geometry and the flap configuration are compared in Figure 23. At the side flap locations (90° and 270° azimuth angle) the torque per blade is lower, compared to the original nacelle geometry. The wind is stagnating behind the flaps due to the blockage. Therefore, a drag force is acting on the blade sections passing the blocked zone. The drag force is counteracting the rotation. Above the flap tips, the flow is accelerated due to the displacement effect. Therefore, higher torque acts on the blade sections passing above the flap tips. Higher flow acceleration is observed at the top flap. Therefore, the torque increases out weight the drag force at the top flap’s location (0° azimuth angle).

In the blank spaces between the flaps, no blockage is introduced by the flaps and the displacement effect to the flaps’ side causes the flow to accelerate. At the azimuth angles related to the blank spaces (45° and 315° azimuth angle), the blade experiences a 3% higher torque. On the downside of the turbine (90° - 270° azimuth angle), the flow acceleration leads to increase turbine torque by 1%. At 180° azimuth angle, the blade is passing through the tower wake. Therefore, a rapid decrease in turbine torque is observed. The minimum of the torque is lifted by 1%.

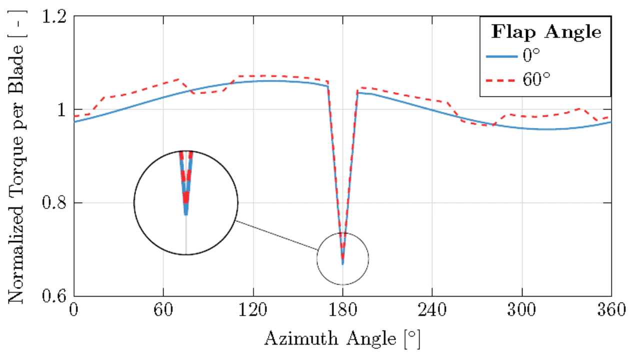

Figure 23: Effect of flaps on the azimuthal variation of torque per blade at low wind speeds. Torque per blade is normalised by mean torque per blade without flaps. wind speed is 6m/s.

The same observations are made at the rated wind speed of 11 m/s shown in Figure 24. But the magnitude of the changes introduced by the flaps is smaller. In the blank space between the flaps, the torque increase is 2%. Inner blade sections are loaded higher at low wind speeds. Therefore, it can be concluded that the flow accelerating effects of the flaps are more substantial at low wind speeds.

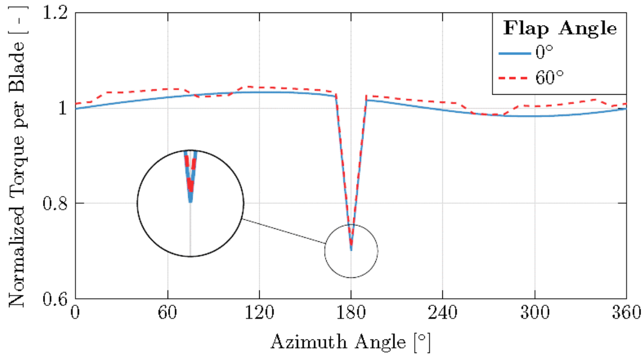

Figure 24: Effect of flaps on the azimuthal variation of torque per blade at low wind speeds. Torque per blade is normalized by mean torque per blade without flaps. wind speed is 11m/s.

The activation of the flaps amplifies the wind turbine's power output. The changes in the torque per blade introduced by the flaps result in an increased power coefficient. In Figure 25 relative increases in the power coefficient, C_P at different wind speeds is shown. At wind speeds higher than 6 m/s a flap angle of 75° is optimal in terms of the power coefficient. From 6-10 m/s the power coefficient increase with the 75° flaps is 1.6%. A lower power coefficient is observed at higher wind speeds. The relative increase at 11 m/s and 12 m/s is 1.3% and 1.2%, respectively.

The higher flap angles do not necessarily lead to a higher power coefficient. As explained in the torque consideration the drag of the inner blade section equilibrates the torque increase due to the flow acceleration. Therefore, with a flap angle of 85° a lower power coefficient is returned and at wind speeds smaller than 6 m/s the maximum power coefficient improvement is gained with the 40° flaps. It is worth noting that the power coefficient improvement is 2.8% at 4 m/s (cut-in wind speed).

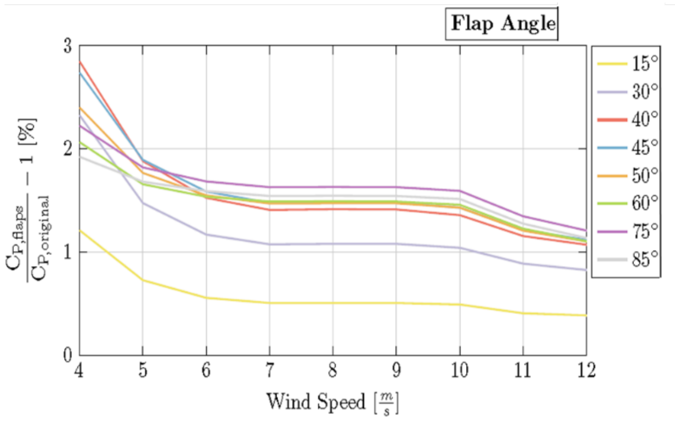

Figure 25: Relative increase in power coefficient C_P by various flap angles

The power coefficient's increase provoked by the installation of flaps is accompanied by an increase in the thrust acting on the turbine. The relative increase in the thrust coefficient is shown in Figure 26. On the contrary to the power coefficient, the thrust coefficient increases with both; flap angle and wind speed. The thrust coefficient increases by 0.5% in the simulations with the 15° flaps but the 75° flaps introduce a 2% and 3.3% increase at 4 m/s and 12 m/s, respectively.

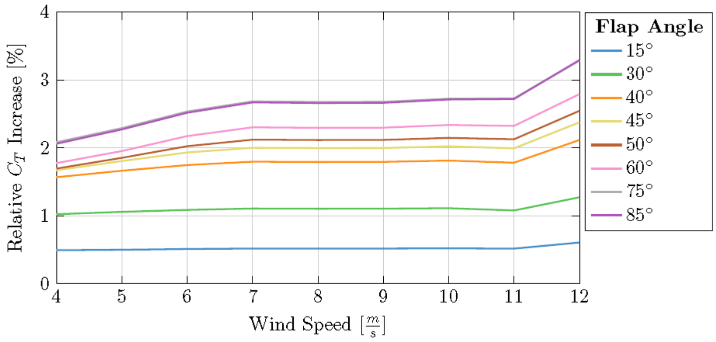

Figure 26: Relative increase in thrust coefficient C_T by various flap angles

The thrust coefficient's increase relates to the flap's aerodynamic drag. In Figure 27 the contribution of the 45° flaps to the additional thrust is shown. The simulations highlight, that 77% of the additional thrust is generated by the drag force acting on the flaps at 4 m/s. At higher wind speeds the flaps' contribution to the drag further increases. It measures 97% at 12 m/s. The additional rotor thrust decreases because of the flaps' displacement effect.

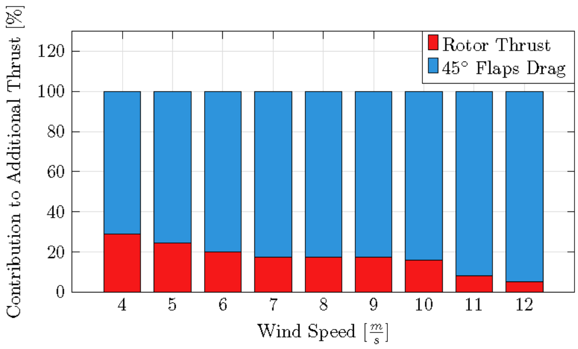

Figure 27: Thrust increase contribution for 45° flap angle.

With a flap angle of 60°, less than 10% of the thrust increase is due to the rotor thrust as shown in Figure 28. At wind speeds of 11 m/s and 12 m/s, the flaps' displacement effect leads to lower rotor thrust. At 11 m/s the rotor thrust is 1% lower compared to simulations without flaps.

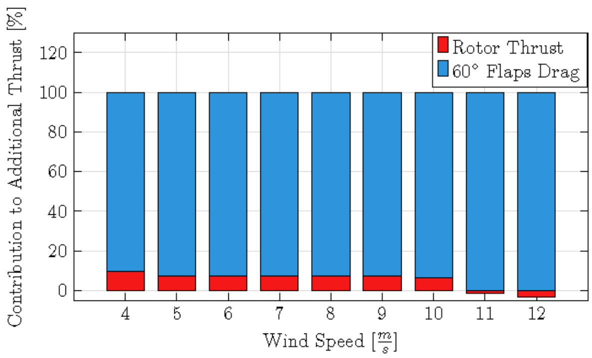

Figure 28: Thrust increase contribution for 60° flap angle.

The quantification of yaw stability is shown in Figure 29. It is indicated that the yaw stability coefficient is increased by increasing the flap angle.

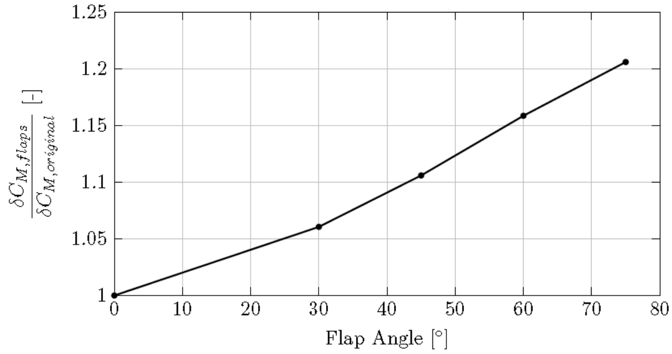

Figure 29: Changes in yaw stability introduced by flaps at rated wind speed.

A decrease in the rotor torque variance is introduced by the flaps. In Figure 30 the rotor torque for various flap configurations is plotted for one revolution. The simulated torque variance is quantified in Figure 31. The results show that the flaps reduce torque variance. With 85° flaps the reductions are 0.9% and 0.2% at 4 m/s and 11 m/s, respectively.

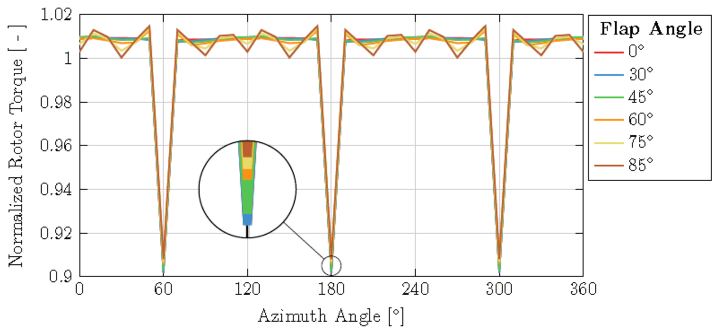

Figure 30: Azimuthal changes in rotor torque at rated wind speed.

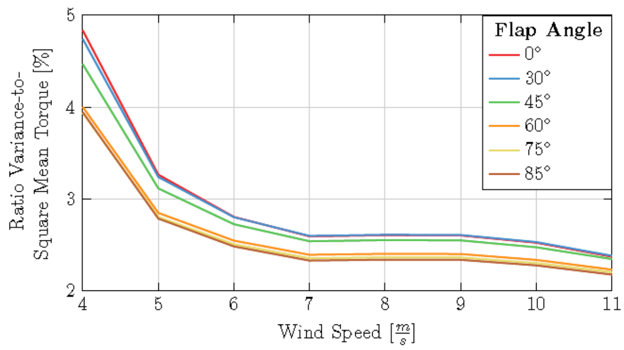

Figure 31: Changes in torque variance.

The simulations show that the activation of the flaps improves the wind turbine's power output. Additionally, the yaw stability is increased. However, these effects are accompanied by an increased thrust. The trends in the 'quasi-steady' variance of the rotor torque can be stated: The rotor torque's variance decreases with increasing flap angle.

4.2 Experimental Results

4.2.1 Upwind configuration

4.2.1.1 Thrust and Power

Figure 32 and Figure 33 show the effect of flaps with different angles on thrust and power coefficient for the case of zero, ±8°, and ±16° yaw angles for the upwind configuration. In Figure 32 and Figure 33, the thrust and power coefficients are normalised by the thrust and power coefficients for no yaw and no flap (C_{T00} and C_{P00}) for the upwind configuration. The angles of flaps are 0°, 30°, 45°, and 60°. It can be seen in Figure 33 that the peak power is achieved with no flap for all yaw angles of zero, ±8°, and ±16° indicating that flaps do not improve turbine power for all yaw angles. The flaps with angles of 30°, 45°, and 60° decrease the turbine power by 0.3%, 3.6%, and 10.4%, respectively for zero yaw angle compared to the case with no flap. Figure 32 shows that the trends in the rotor thrust do not follow the trends seen in the turbine power. The flaps with an angle of 30° do not change turbine thrust for zero yaw angle. The flaps with an angle of 45° increase the turbine thrust by 0.3% while the turbine thrust is reduced by 0.7% with a flaps angle of 60° for zero yaw angle compared to the case with no flap.

The effect of flaps with different angles on the ratio of turbine power and thrust coefficient (C_P/C_T) is shown in Figure 34 for the case of zero, ±8°, and ±16° yaw angles for the upwind configuration. The ratio of turbine power and thrust coefficient (C_P/C_T) can represent the amount of wind power extracted by the turbine per unit of rotor thrust. It can be seen in Figure 34 that flaps with angles of 30°, 45°, and 60° reduce the ratio of turbine power and thrust coefficient (C_P/C_T) for all yaw angles for the upwind configuration. The turbine C_P/C_T ratio is reduced by 0.3%, 3.9%, and 9.8% using flaps with angles of 30°, 45°, and 60°, respectively for 0° yaw angle compared to the case with no flap. In the case of -16° (and +16°) yaw angle, flaps with angles of 30°, 45°, and 60° reduce the C_P/C_T ratio by 1.9% (2.0%) and 4.9% (6.8%), and 12.1% (11.8%), respectively compared to the case with no flap.

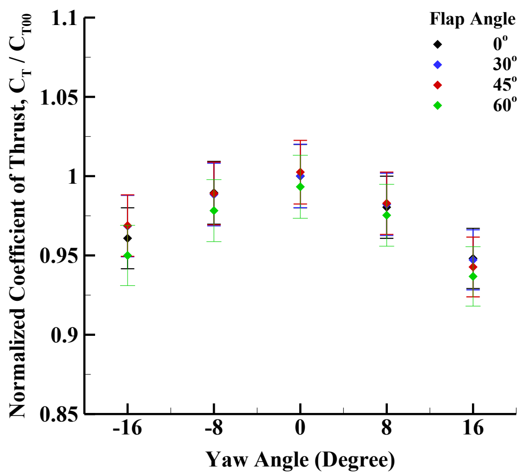

Figure 32. Effect of flaps on rotor thrust for yaw angle of 0°, ±8°, and ±16° for upwind configuration.

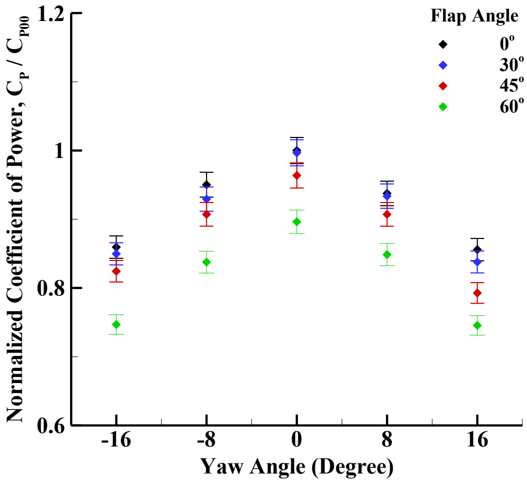

Figure 33. Effect of flaps on turbine power for yaw angle of 0°, ±8°, and ±16° for upwind configuration.

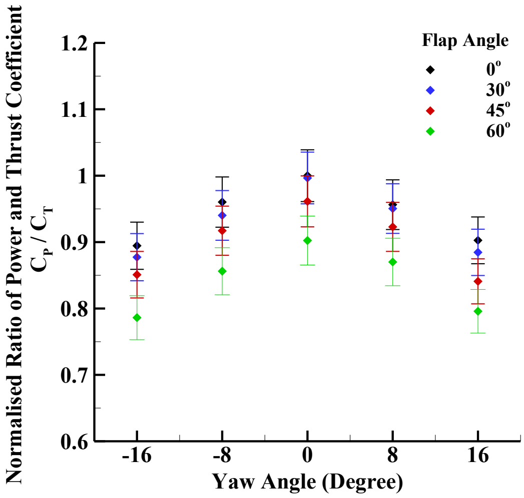

Figure 34. Effect of flaps on C_P/C_T ratio for yaw angle of 0°, ±8°, and ±16° for upwind configuration.

4.2.1.2 Unsteady Loads

In order to investigate the effect of flaps on wind turbine fatigue loads, a full phase domain analysis is done using the ensemble averaging technique on the variation of rotor thrust and torque during wind turbine operation. The low-frequency fluctuations or amplitude ratio of major loads is determined from the ratio of the difference between maximum and minimum loads and the average load during a rotor revolution. The thrust and torque for all yaw angles of 0°, ±8°, and ±16° are normalised by the respective mean for no yaw and no flap for each configuration. The total unsteadiness of rotor thrust and torque is determined by integrating the power spectral density of the measured unsteady loads. In the case of ‘1P’, ‘3P’, ‘Rotor Vortex’ variances the bandwidths of integration are ±10% of the rotational speed frequency, blade passing frequency, and vortex-shedding frequency, respectively, and the ‘Others’ variance is determined from the integral outside these bandwidths. The total unsteadiness of thrust and torque for all yaw angles of 0°, ±8°, and ±16° are also normalised by the respective total unsteadiness for no yaw and no flap for each configuration.

Figure 35 and Figure 36 show the effect of flaps with angles of 0°, 30°, 45°, and 60° on the variations of rotor thrust and torque, respectively during a rotor revolution in the case of zero yaw angle for the upwind configuration. As it is shown in Table 5, flaps with angles of 30° and 45° reduce the amplitude ratio of rotor thrust by 9% and 1%, respectively compared to the case with no flap while the amplitude ratio of rotor thrust is increased by 5% with flaps angle of 60°. It also can be seen that flaps with angles of 30°, 45°, and 60° increase the amplitude ratio of rotor torque by 10%, 18%, and 24%, respectively for zero yaw angle compared to the case with no flap.

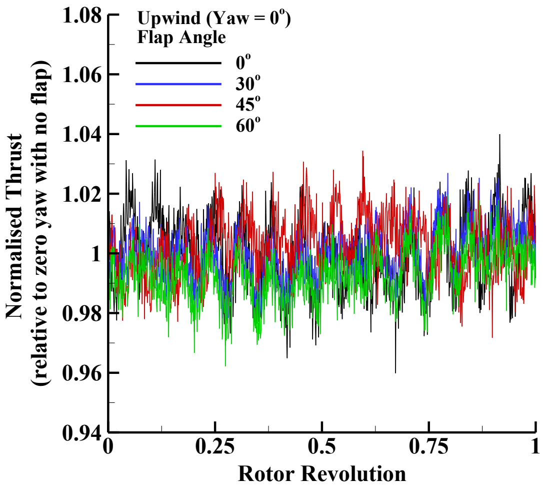

Figure 35. Effect of flaps on the variation of rotor thrust during a rotor revolution at zero yaw angle for upwind configuration.

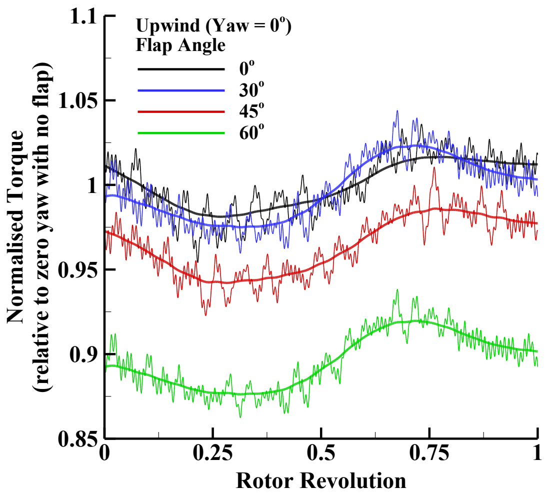

Figure 36. Effect of flaps on the variation of rotor torque during a rotor revolution at zero yaw angle for upwind configuration.

Table 5. Effect of flaps on the amplitude ratio of rotor thrust and torque during a rotor revolution at zero yaw angle for upwind configuration.

Flap angle	Normalised amplitude ratio (relative to zero yaw angle with no flap)	
	Thrust	Torque
0°	1	1
30°	0.91	1.10
45°	0.99	1.18
60°	1.05	1.24

Figure 37 and Figure 38 show the effect of flaps with angles of 0°, 30°, 45°, and 60° on the variance of rotor thrust and torque, respectively in the case of zero yaw angle for the upwind configuration. The contributions of each part are normalised by the value for a yaw angle of 0° with no flap. It is evident that flaps with angles of 30° and 45° reduce the total unsteadiness of rotor thrust by 17% and 1%, respectively compared to the case with no flap while flaps with an angle of 60° do not change the total unsteadiness of the rotor thrust at a yaw angle of 0°. It can be seen in Figure 38 that flaps with angles of 30°, 45°, and 60° increase the total unsteadiness of rotor torque by 9%, 17%, and 46%, respectively for zero yaw angle compared to the case with no flap.

Figure 39 and Figure 40 show the effect of flaps with angles of 0°, 30°, 45°, and 60° on the amplitude ratio and the total unsteadiness of rotor thrust, respectively during a rotor revolution in the case of ±8° and ±16° yaw angles for the upwind configuration. It can be seen in Figure 39 that flaps with an angle of 30° reduce the amplitude ratio of rotor thrust by 18%, 5%, 19%, and 20%, respectively for all yaw angles of -16°, -8°, +8°, and +16° compared to the case with no flap. Flaps with angles of 45° and 60° reduce the amplitude ratio of rotor thrust for positive yaw angles while increasing the amplitude ratio of rotor thrust for negative yaw angles compared to the case with no flap.

It is shown in Figure 40 that flaps with angles of 30° (and 45°) reduce the total unsteadiness of rotor thrust by 8% (3%), 4% (9%), 21% (21%), and 9% (3%), respectively for all yaw angles of -16°, -8°, +8°, and +16° compared to the case with no flap. It can be seen that flaps with an angle of 60° reduce the total unsteadiness of rotor thrust for yaw angles of ±8° while increasing the total unsteadiness of rotor thrust for yaw angles of ±16° compared to the case with no flap.

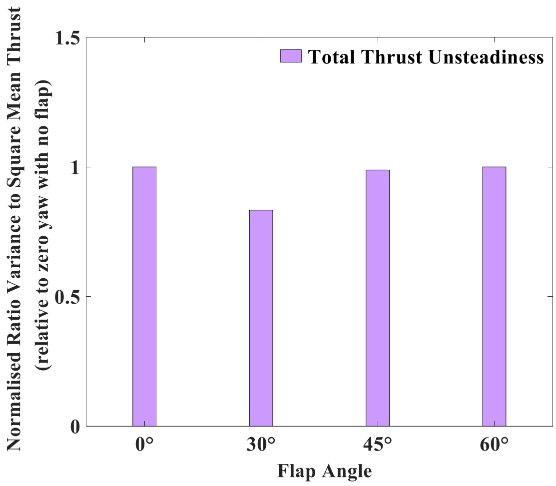

Figure 37. Effect of flaps on the total unsteadiness of rotor thrust during a rotor revolution at zero yaw angle for upwind configuration.

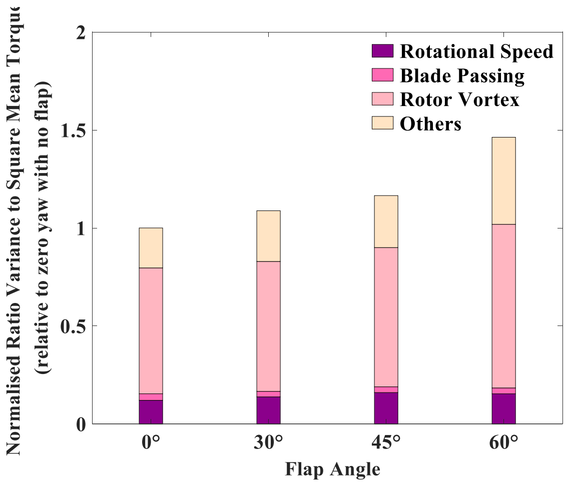

Figure 38. Effect of flaps on the total unsteadiness of rotor torque during a rotor revolution at zero yaw angle for upwind configuration.

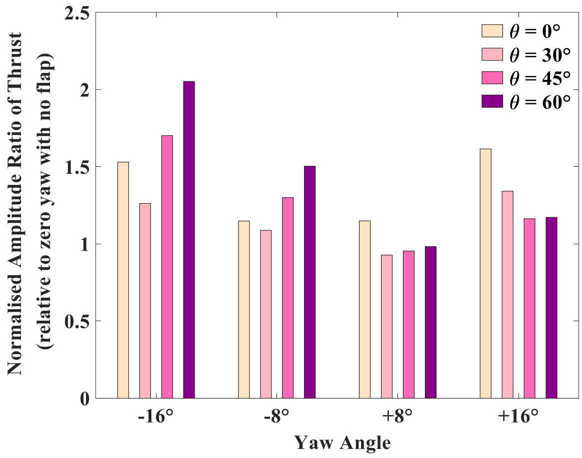

Figure 39. Effect of flaps on the amplitude ratio of rotor thrust during a rotor revolution at ±8° and ±16° yaw angles for upwind configuration.

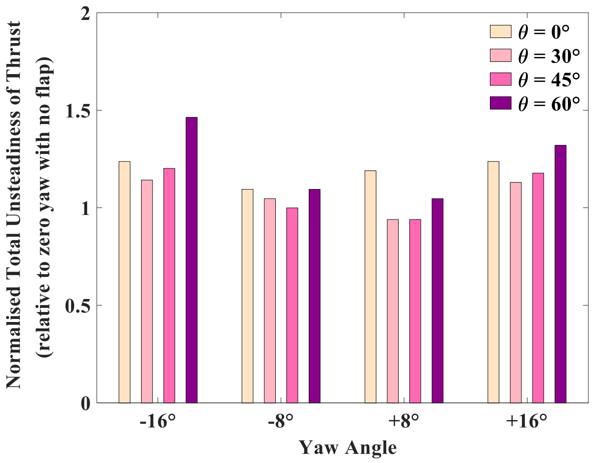

Figure 40. Effect of flaps on the total unsteadiness of rotor thrust during a rotor revolution at ±8° and ±16° yaw angles for upwind configuration.

Figure 41 and Figure 42 show the effect of flaps with angles of 0°, 30°, 45°, and 60° on the amplitude ratio and the total unsteadiness of rotor torque, respectively during a rotor revolution in the case of ±8°

and ±16° yaw angles for the upwind configuration. It can be seen in Figure 41 that flaps with an angle of 30° reduce the amplitude ratio of rotor torque by 3%, 19%, and 10%, respectively for yaw angles of -16°, +8°, and +16° while increasing the amplitude ratio of rotor torque by 6% for yaw angle of -8° compared to the case with no flap. Flaps with an angle of 45° reduce the amplitude ratio of rotor torque for positive yaw angles while increasing the amplitude ratio of rotor torque for negative yaw angles. It also can be seen that flaps with and angle of 60° increase the amplitude ratio of rotor torque for all yaw angles of ±8° and ±16° compared to the case with no flap.

It is shown in Figure 42 that flaps with an angle of 30° reduce the total unsteadiness of rotor torque by less than 1% and 7%, respectively for yaw angles of -16° and +8° while increasing the total unsteadiness of rotor torque by 9% and 8%, respectively for yaw angles of -8° and +16° compared to the case with no flap. Flaps with an angle of 45° increase the total unsteadiness of rotor torque for all yaw angles except yaw angle of +8° where the total unsteadiness of rotor torque is reduced by 6%. However, flaps with an angle of 60° increase the total unsteadiness of rotor torque for all yaw angles of ±8° and ±16° compared to the case with no flap.

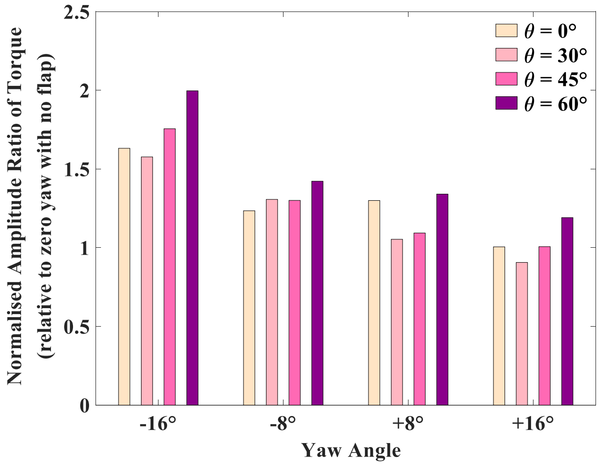

Figure 41. Effect of flaps on the amplitude ratio of rotor torque during a rotor revolution at ±8° and ±16° yaw angles for upwind configuration.

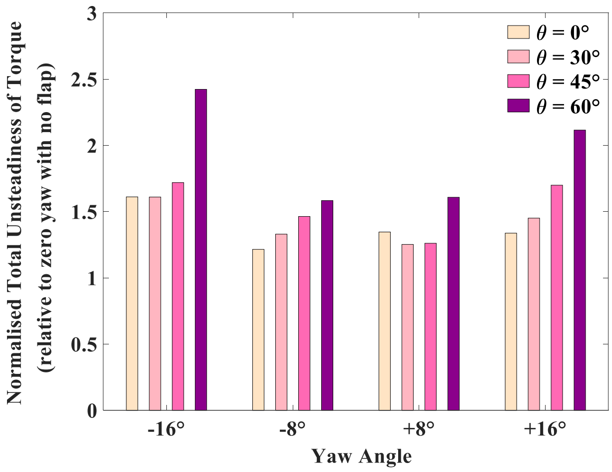

Figure 42. Effect of flaps on the total unsteadiness of rotor torque during a rotor revolution at ±8° and ±16° yaw angles for upwind configuration.

4.2.1.3 Blade Cumulative Fatigue Damage

Table 6 shows the effect of flaps on the blade cumulative damage for the upwind configuration. The case of zero yaw angle with no flap is considered as the reference case with a safety factor of 2 applied following IEC wind turbine standards [15] for blade fatigue life analysis.

It is evident that the blade cumulative damage fraction is reduced by 48% and 7% with flap angles of 30° and 45°, respectively while flaps with an angle of 60° increase the blade cumulative damage fraction by 29% at zero yaw angle. It can be seen that flaps with an angle of 30° reduce the blade cumulative damage fraction for all yaw angles of ±8° and ±16° compared to the case with no flap while flaps with angles of 45° and 60° reduce the blade cumulative damage fraction only for positive yaw angles of +8° and +16°.

It should be noted that in the case of no flap, the blade cumulative damage fraction is increased by 1075%, 129%, 109%, and 1380%, respectively for yaw angles of -16°, -8°, +8°, and +16°. In the case of +8° yaw angle, using flaps compensates for the adverse effect of yaw misalignment on the blade cumulative fatigue damage.

Table 6. Effect of flaps on the blade cumulative fatigue damage for upwind configuration.

Flap angle	Change of blade cumulative damage fraction (%) (relative to zero yaw angle with no flap)				
	Yaw = -16°	Yaw = -8°	Yaw = 0°	Yaw = +8°	Yaw = +16°
0°	+1075	+129	0	+109	+1379
30°	+247	+58	-48	-22	+327
45°	+2470	+413	-7	-38	+58
60°	+7313	+1130	+29	-29	+58

4.2.1.4 Yaw Stability

Figure 43 shows the effect of flaps on the yaw twisting moment coefficients for yaw angles of zero, ±8°, and ±16° for the upwind configuration. The yaw stability coefficient is given as the difference of the coefficient of twisting moments with and without yaw (C_M-C_{M0}) are normalised by the coefficient of the twisting moment at a yaw angle of 0° with no flap (CM00) and divided by yaw angle change ($\Delta C_M/\Delta\beta$ = $[(C_M-C_{M0})/\ C_{M00}]/[\Delta\beta]$). Negative coefficients indicate yaw stability. This means that for a positive/negative incremental change of the yaw angle, the rotor experiences an incremental decrease/increase in the yaw moment, which will increase/reduce the incremental change of the yaw angle and leads to align the wind turbine to the wind direction [6].

Table 7 shows the effect of flaps on the yaw stability coefficient for the upwind configuration. Firstly, for no flap and ±16° yaw angles, the upwind configuration is not generally stable and the yaw stability is more for positive yaw angles in comparison to negative. Secondly, it can be seen that for a negative yaw angle of -16°, flaps with an angle of 30° increase yaw stability as the yaw stability coefficient is smaller than for the no flap condition. It is evident that in the case of a positive yaw angle of +16°, flaps do not improve the wind turbine yaw stability.

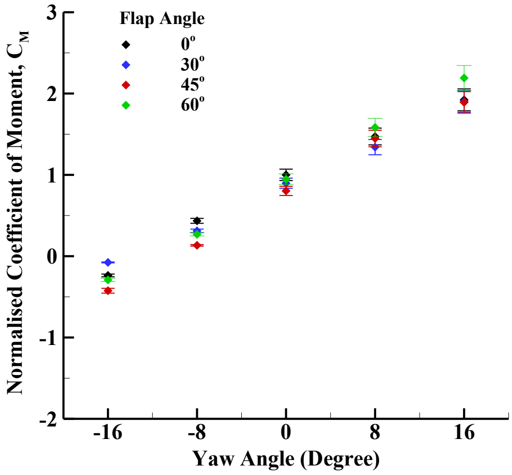

Figure 43. Effect of flaps on yaw twisting moment for yaw angle of 0°, ±8°, and ±16° for upwind configuration.

Table 7. Effect of flaps on the yaw stability coefficient for upwind configuration.

Flap angle	Normalised yaw stability coefficient ($\Delta C_M/\Delta\beta$)	
	Yaw = -16°	Yaw = +16°
0°	0.08	0.06
30°	0.06	0.06
45°	0.08	0.07
60°	0.08	0.08

4.2.1.5 Recommended Flap for Upwind Configuration

Table 8 shows the recommended flap for the upwind configuration. It can be seen that flaps with an angle of 30° decrease the blade cumulative fatigue damage for all yaw angles and reduced the rotor torque unsteady loads for yaw angles of +8° and ±16° where there is no adverse effect on the turbine yaw stability. Therefore, it is recommended to use flaps with an angle of 30° for yaw angles of +8° and ±16° while a marginal power reduction should be considered. It is worth noting that in the case of zero and -8° yaw angles, flaps with an angle of 30° decrease the blade cumulative fatigue damage while increasing the rotor torque unsteady loads with a marginal reduction in turbine power. Therefore, it is not recommended to use flaps in the case of zero and -8° yaw angles, and the control system should be commanded to close the flaps.

Table 8. Recommended flap for upwind configuration.

Yaw angle	Flap angle	Effect of flaps on the turbine parameters (relative to the case with no flap for each yaw angle)						Conclusion (*)
		C_P	C_T	C_P/C_T	Blade cumulative fatigue damage	Torque unsteady loads	Yaw stability	
0°	30°	-0.3%	0%	-0.3%	-48%	Increased	-	×
-16°	30°	-1.1%	+0.8%	-1.9%	-70%	Reduced	Improved	+
-8°	30°	-2.2%	-0.1%	-2.1%	-31%	Increased	Improved	×
+8°	30°	-0.4%	+0.2%	-0.6%	-63%	Reduced	No change	+
+16°	30°	-2.1%	-0.1%	-2.0%	-71%	Reduced	No change	+

(*)
++ Highly recommended
+ Recommended (marginal power reduction)
× Not recommended

4.2.2 Downwind configuration

4.2.2.1 Thrust and Power

Figure 44 and Figure 45 show the effect of flaps with different angles on thrust and power coefficient for the case of zero, ±8°, and ±16° yaw angles for the downwind configuration. In Figure 44 and Figure 45, the thrust and power coefficients are normalised by the thrust and power coefficients for no yaw and no flap (C_{T00} and C_{P00}) for the downwind configuration. The angles of flaps are 0°, 30°, 45°, and 60°. It can be seen in Figure 45 that the peak power is achieved with a flaps angle of 60° for all yaw angles of zero, ±8°, and ±16°. The flaps with angles of 30°, 45°, and 60° increase the turbine power by 1.5%, 10.7%, and 12.3%, respectively for zero yaw angle compared to the case with no flap. Figure 44 shows that the trends in the rotor thrust follow the trends seen in the turbine power. The flaps with angles of 30°, 45°, and 60° increase the turbine thrust by 2.2%, 6.4%, and 7.6%, respectively for zero yaw angle compared to the case with no flap. It is worth noting that in the case of ±8° yaw angles, flaps with angles of 45° and 60° compensate for the power reduction due to rotor yaw misalignment.

The effect of flaps with different angles on the ratio of turbine power and thrust coefficient (C_P/C_T) is shown in Figure 46 for the case of zero, ±8°, and ±16° yaw angles for the downwind configuration. The ratio of turbine power and thrust coefficient (C_P/C_T) can represent the amount of wind power extracted by the turbine per unit of rotor thrust. It can be seen in Figure 46 that flaps with an angle of 30° reduce the ratio of turbine power and thrust coefficient (C_P/C_T) by 0.7% while flaps with angles of 45° and 60° increase the ratio of turbine power and thrust coefficient (C_P/C_T) by 4.0% and 4.4%, respectively for 0° yaw angle compared to the case with no flap for the downwind configuration. In the case of -8° (and +8°) yaw angle, flaps with angles of 30°, 45°, and 60° increase the C_P/C_T ratio by 11.8% (13.5%) and 13.6% (13.0%), and 15.4% (15.2%), respectively compared to the case with no flap. It is evident that in the case of -16° (and +16°) yaw angle, flaps with angles of 30°, 45°, and 60° increase the C_P/C_T ratio by 18.0% (9.5%) and 16.4% (6.6%), and 15.9% (7.8%), respectively compared to the case with no flap.

It should be noted that only flaps with an angle of 60° compensate for the C_P/C_T reduction due to rotor yaw misalignment in the case of ±8° yaw angles. The C_P/C_T is improved by 0.6% and 1% for -8° and +8° yaw angles, respectively in comparison to the case with no yaw.

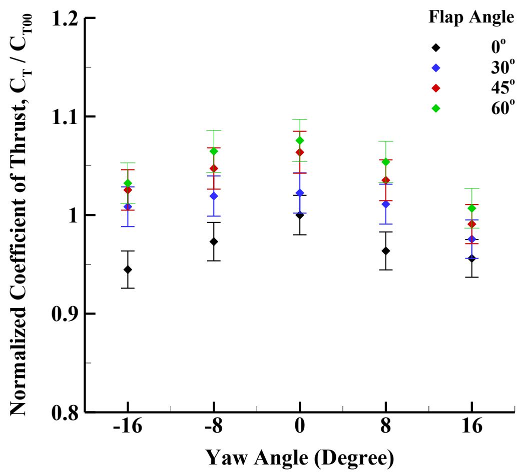

Figure 44. Effect of flaps on rotor thrust for yaw angle of 0°, ±8°, and ±16° for downwind configuration.

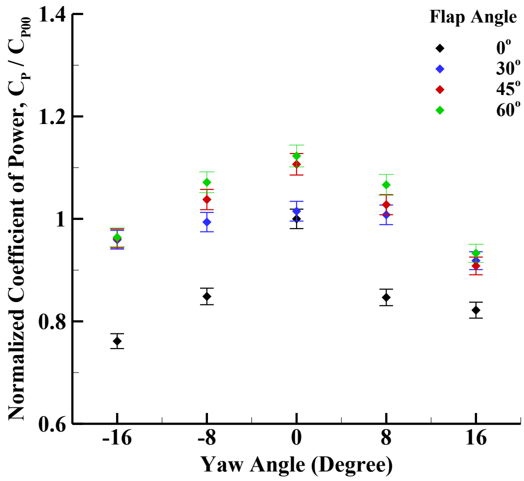

Figure 45. Effect of flaps on turbine power for yaw angle of 0°, ±8°, and ±16° for downwind configuration.

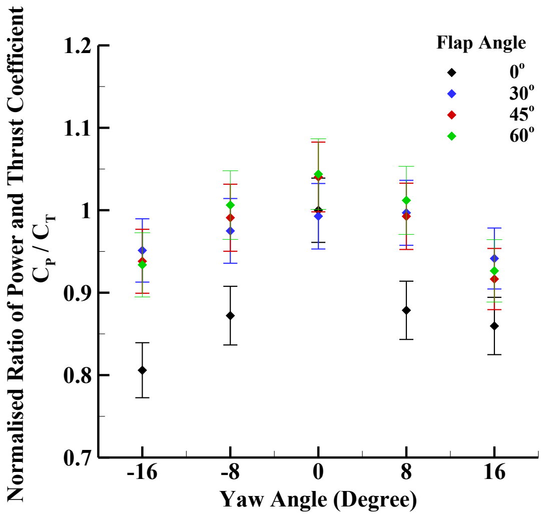

Figure 46. Effect of flaps on C_P/C_T ratio for yaw angle of 0°, ±8°, and ±16° for downwind configuration.

4.2.2.2 Unsteady Loads

Figure 47 and Figure 48 show the effect of flaps with angles of 0°, 30°, 45°, and 60° on the variations of rotor thrust and torque, respectively during a rotor revolution in the case of zero yaw angle for the downwind configuration. As it is shown in Table 9, flaps with angles of 30°, 45°, and 60° reduce the amplitude ratio of rotor thrust by 11%, 17%, and 40%, respectively compared to the case with no flap. It also can be seen that flaps with angles of 30°, 45°, and 60° reduce the amplitude ratio of rotor torque by 27%, 42%, and 59%, respectively for zero yaw angle compared to the case with no flap.

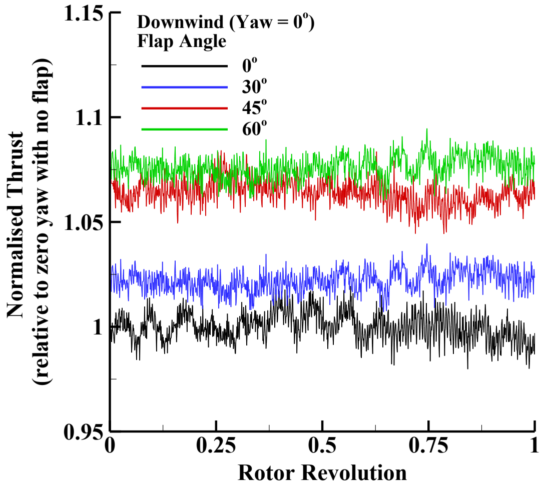

Figure 47. Effect of flaps on the variation of rotor thrust during a rotor revolution at zero yaw angle for downwind configuration.

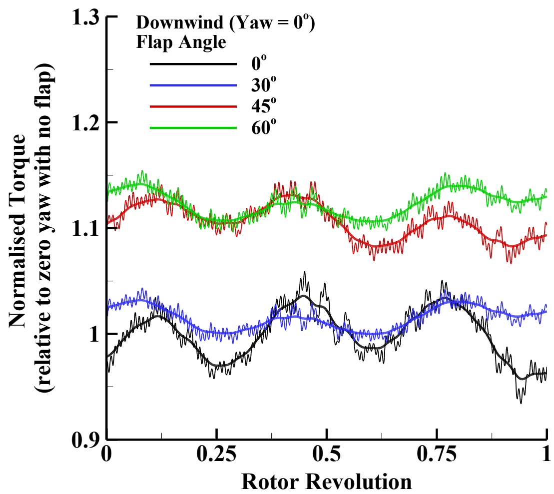

Figure 48. Effect of flaps on the variation of rotor torque during a rotor revolution at zero yaw angle for downwind configuration.

Table 9. Effect of flaps on the amplitude ratio of rotor thrust and torque during a rotor revolution at zero yaw angle for downwind configuration.

Flap angle	Normalised amplitude ratio (relative to zero yaw angle with no flap)	
	Thrust	Torque
0°	1	1
30°	0.89	0.73
45°	0.83	0.58
60°	0.60	0.41

Figure 49 and Figure 50 show the effect of flaps with angles of 0°, 30°, 45°, and 60° on the variance of rotor thrust and torque, respectively in the case of zero yaw angle for the downwind configuration. The contributions of each part are normalised by the value for the case of a yaw angle of 0° with no flap. It is evident that flaps with angles of 30°, 45°, and 60° reduce the total unsteadiness of rotor thrust by 35%, 51%, and 54%, respectively compared to the case with no flap. It can be seen in Figure 50 that flaps with angles of 30°, 45°, and 60° also reduce the total unsteadiness of rotor torque by 41%, 59%, and 68%, respectively for zero yaw angle compared to the case with no flap.

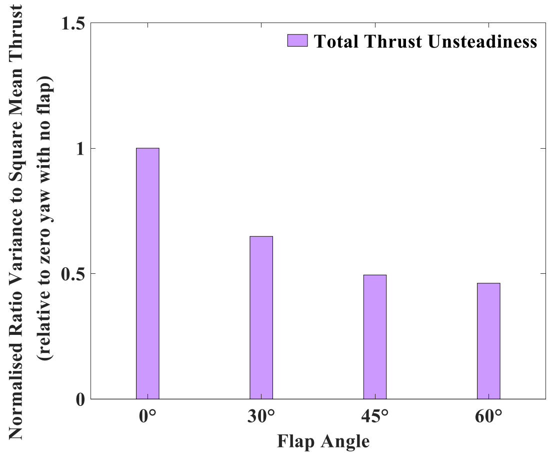

Figure 49. Effect of flaps on the total unsteadiness of rotor thrust during a rotor revolution at zero yaw angle for downwind configuration.

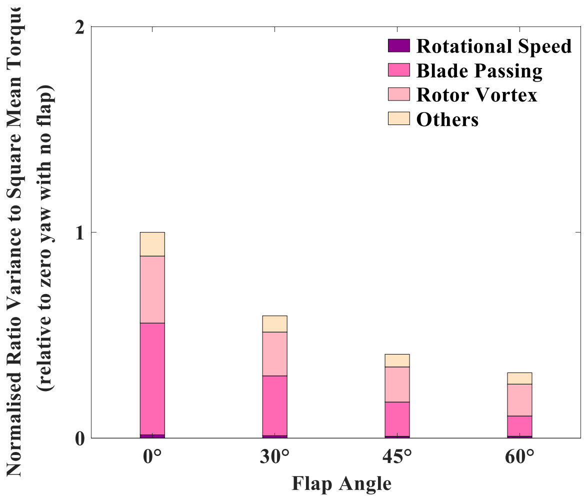

Figure 50. Effect of flaps on the total unsteadiness of rotor torque during a rotor revolution at zero yaw angle for downwind configuration.

Figure 51 and Figure 52 show the effect of flaps with angles of 0°, 30°, 45°, and 60° on the amplitude ratio and the total unsteadiness of rotor thrust, respectively during a rotor revolution in the case of ±8° and ±16° yaw angles for the downwind configuration. It can be seen in Figure 51 that flaps with angles of 30°, 45°, and 60° reduce the amplitude ratio of rotor thrust for all yaw angles compared to the case with no flap. Flaps with an angle of 60° result in the maximum reduction of amplitude ratio of rotor thrust by 35%, 14%, and 38%, respectively for yaw angles of -8°, +8°, and +16° while flaps with an angle of 30° result in the maximum reduction of amplitude ratio of rotor thrust by 27% for -16° yaw angle compared to the case with no flap.

It is shown in Figure 52 that flaps with an angle of 60° result in the maximum reduction of total unsteadiness of rotor thrust by 57%, 63%, 52%, and 28%, respectively for yaw angles of -16°, -8°, +8°, and +16° compared to the case with no flap.

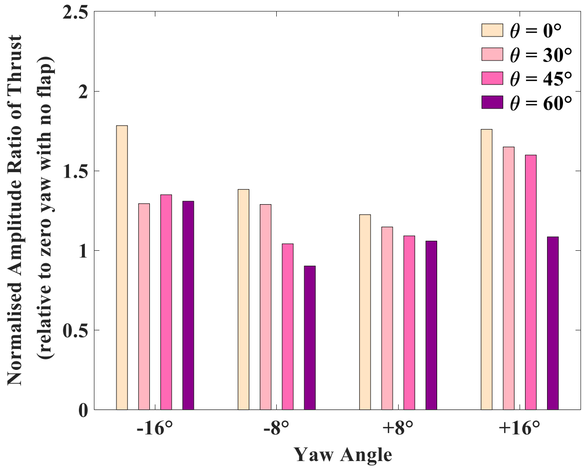

Figure 51. Effect of flaps on the amplitude ratio of rotor thrust during a rotor revolution at ±8° and ±16° yaw angles for downwind configuration.

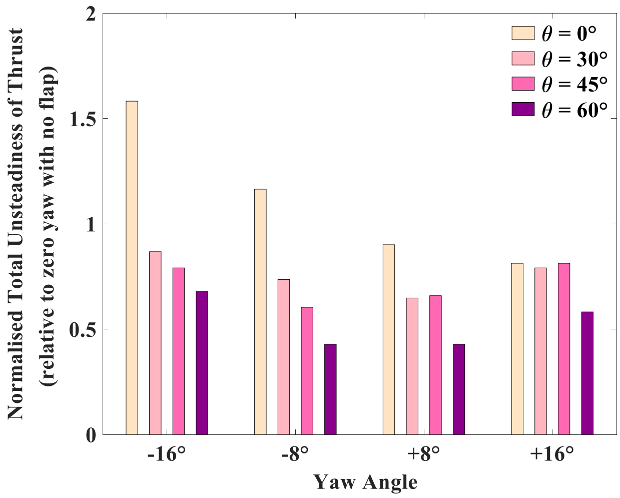

Figure 52. Effect of flaps on the total unsteadiness of rotor thrust during a rotor revolution at ±8° and ±16° yaw angles for downwind configuration.

Figure 53 and Figure 54 show the effect of flaps with angles of 0°, 30°, 45°, and 60° on the amplitude ratio and the total unsteadiness of rotor torque, respectively during a rotor revolution in the case of ±8° and ±16° yaw angles for the downwind configuration. It can be seen in Figure 53 that flaps with angles of 30°, 45°, and 60° reduce the amplitude ratio of rotor torque for all yaw angles compared to the case with no flap. Flaps with an angle of 60° result in the maximum reduction of amplitude ratio of rotor torque by 26% and 29%, respectively for yaw angles of -8° and +8° while flaps with an angle of 45° (and 30°) result in the maximum reduction of amplitude ratio of rotor torque by 20% (17%) for -16° (+16°) yaw angle compared to the case with no flap.

It is shown in Figure 54 that flaps with an angle of 60° result in the maximum reduction of total unsteadiness of rotor torque by 56%, 54%, and 13%, respectively for yaw angles of -8°, +8°, and +16° compared to the case with no flap while flaps with an angle of 45° result in the maximum reduction of total unsteadiness of rotor torque by 50% for -16° yaw angle.

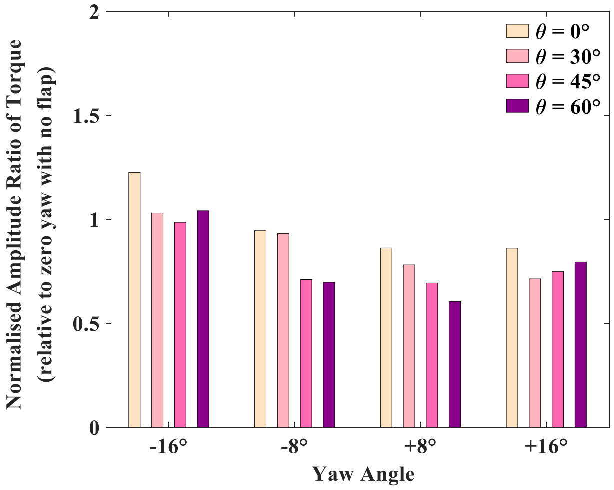

Figure 53. Effect of flaps on the amplitude ratio of rotor torque during a rotor revolution at ±8° and ±16° yaw angles for downwind configuration.

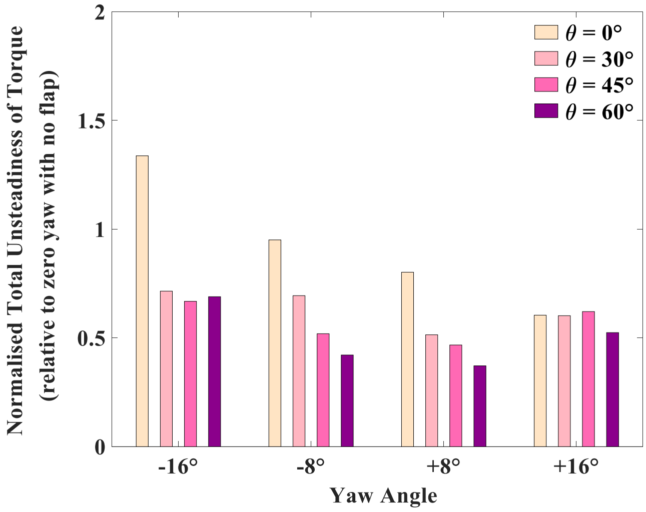

Figure 54. Effect of flaps on the total unsteadiness of rotor torque during a rotor revolution at ±8° and ±16° yaw angles for downwind configuration.

4.2.2.3 Blade Cumulative Fatigue Damage

Table 10 shows the effect of flaps on the blade cumulative damage for the downwind configuration. The case of zero yaw angle with no flap is considered as the reference case with a safety factor of 2 applied as in the case of the upwind configuration.

It is evident that flaps with angles of 30°, 45°, and 60° reduce the blade cumulative damage fraction by 45%, 48%, and 94%, respectively for 0° yaw angle. It can be seen that for all yaw angles except -16°, flaps with an angle of 60° result in the maximum reduction of blade cumulative damage fraction while in the case of -16°, flaps with an angle of 30° result in the maximum reduction of blade cumulative damage fraction.

It should be noted that in the case of no flap, the blade cumulative damage fraction is increased by 2654%, 561%, 169%, and 2654%, respectively for -16°, -8°, +8°, and +16° yaw angles.

Table 10. Effect of flaps on the blade cumulative fatigue damage for downwind configuration.

Flap angle	Change of blade cumulative damage fraction (%) (relative to zero yaw angle with no flap)				
	Yaw = -16°	Yaw = -8°	Yaw = 0°	Yaw = +8°	Yaw = +16°
0°	+2654	+561	0	+169	+2654
30°	+489	+531	-45	+169	+2088
45°	+812	+100	-48	+145	+1942
60°	+694	-9	-94	+134	+82

4.2.2.4 Yaw Stability

Figure 55 and Table 11 show the effect of flaps on the yaw twisting moment coefficients and on the yaw stability coefficient, respectively for yaw angles of zero, ±8°, and ±16° for the downwind configuration. Firstly, for no flap and ±16° yaw angles, the downwind configuration is generally stable and the yaw stability is more for positive yaw angles in comparison to negative. Secondly, it can be seen that for a negative yaw angle of -16°, flaps with all angles increase the wind turbine yaw stability. It is evident that in the case of +16° yaw angle, flaps with angles of 45° and 60° increase the wind turbine yaw stability while flaps with an angle of 30° decrease the wind turbine yaw stability.

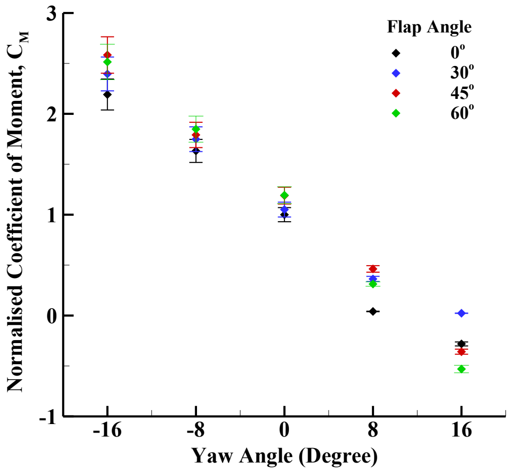

Figure 55. Effect of flaps on yaw twisting moment for yaw angle of 0°, ±8°, and ±16° for downwind configuration.

Table 11. Effect of flaps on the yaw stability coefficient for downwind configuration.

Flap angle	Normalised yaw stability coefficient ($\Delta C_M/\Delta\beta$)	
	Yaw = -16°	Yaw = +16°
0°	-0.07	-0.08
30°	-0.08	-0.06
45°	-0.09	-0.10
60°	-0.08	-0.11

4.2.2.5 Reduction in Cut-in Speed

Using flaps decreases the cut-in speed, and therefore increases the turbine annual energy yield by increasing the range of power generation. Table 12 shows the effect of flaps on cut-in speed for a zero yaw angle for the downwind configuration. It can be seen that flaps with angles of 30°, 45°, and 60° reduce the wind turbine cut-in speed by 0.5%, 3.4%, and 3.9%, respectively for zero yaw angle.

Table 12. Effect of flaps on the cut-in speed for zero yaw angle for downwind configuration.

Flap angle	Change in turbine cut-in speed (relative to zero yaw angle with no flap)
0°	0%
30°	-0.5%
45°	-3.4%
60°	-3.9%

4.2.2.6 Recommended Flap for Downwind Configuration

Table 13 shows the recommended flap for the downwind configuration. The maximum reduction in the blade cumulative fatigue damage and the maximum improvement in the ratio of turbine power and turbine thrust (C_P/C_T) are considered as the criteria for the recommended flap.

Table 13. Recommended flap for downwind configuration.

Yaw angle	Flap angle	Effect of flaps on the turbine parameters (relative to the case with no flap for each yaw angle)						Conclusion (*)
		C_P	C_T	C_P/C_T	Blade cumulative fatigue damage	Torque unsteady loads	Yaw stability	
0°	60°	+12.3%	+7.6%	+4.4%	-94%	Reduced	-	+++
-16°	30°	+26.0%	+6.8%	+18%	-79%	Reduced	Improved	+++
	60°	+26.6%	+9.3%	+15.9%	-71%	Reduced	Improved	++
-8°	60°	+26.2%	+9.4%	+15.4%	-86%	Reduced	Improved	+++
+8°	60°	+26.0%	+9.4%	+15.2%	-13%	Reduced	Improved	+++
+16°	30°	+11.8%	+2.0%	+9.5%	-21%	Reduced	Reduced	++
	60°	+13.5%	+5.3%	+7.8%	-93%	Reduced	Improved	+++

(*)
+++ Highly recommended
++ Recommended
+ Can be used
× Not recommended

Based on the criteria, it is highly recommended to use flaps with an angle of 60° for yaw angles of 0°, ±8°, and +16° and flaps with an angle of 30° for -16° yaw angle for the downwind configuration.

4.3 Theoretical Explanations

As described in section 3.3, generally, the inner spans of wind turbine blades:

- Experience low relative velocities and high incidence angles (compared to the outer spans).
- Have low lift/drag ratio (even < 1).
- Generally, do not contribute to generating power, but generate thrust.

Therefore, blocking the inner spans (<20% span) pushes the flow towards outer spans (>20% span) which have higher lift/drag coefficients. On the other hand, flaps block the inner spans which do not contribute to power generation, but nevertheless generate thrust and unsteady loads as shown in Figure 56. Nevertheless, the increased flow over the outer spans may contribute to power generation, and thus improved turbine power and efficiency are expected.

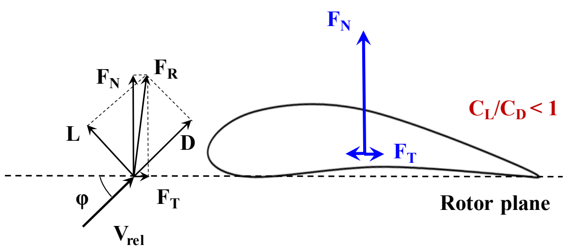

(a)

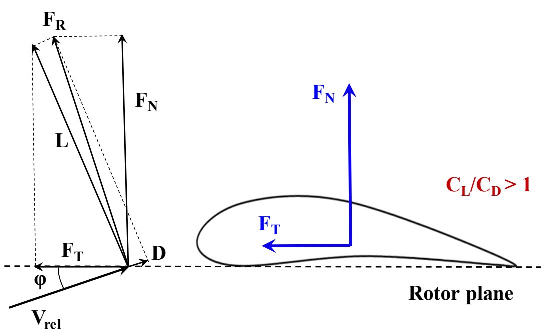

(b)

Figure 56. Loads diagram for a) inner and b) outer spans blade sections

Consequently, the effectiveness of the optimised nacelle using flaps on upwind and downwind configurations which are shown schematically in Figure 57 can be explained as follows:

➢ Upwind configuration:

- Increased downstream velocity (and the slowed down upstream velocity) leads to a marginally decrease in turbine power (following from the turbine Euler equation) and consequently may marginally increase the torque.
- Slow down of flow on inner spans with lower lift/drag ratios leads to mitigated thrust on inner spans.

➢ Downwind configuration:

- Increased upstream velocity leads to improved turbine power (following from the turbine Euler equation).
- Pushing the flow to outer spans with higher lift/drag ratios leads to mitigation of unsteady loads (thrust and torque) that are generated on inner spans.

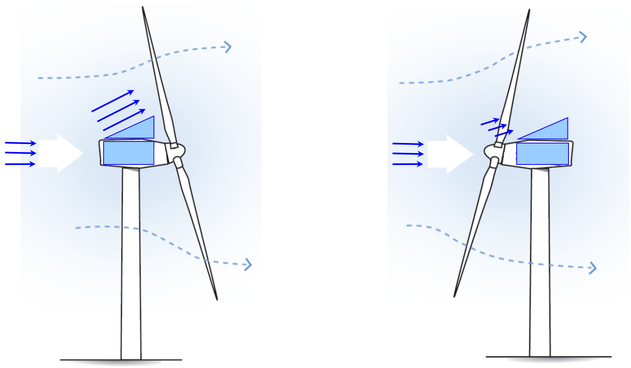

Figure 57. Schematic of the effectiveness of flaps on upwind and downwind configurations.

5 Concluding Remarks

A novel comparative study of the effectiveness of optimised nacelle using flaps on fatigue loads alleviation and performance improvement in both upwind and downwind configurations has been conducted. The experiments are accomplished on a scale model of a commercial 2MW wind turbine that has a rotor tilt of 8°, and a cone angle of 5°. The model is instrumented with tower root-mounted strain gauges and a custom-built in-line torque meter from which time histories of thrust, bending moment, twisting moment, and torque are measured. The effectiveness of different flaps angles in alleviating fatigue loads and improve turbine power is assessed. An extensive full phase domain analysis of the measured load variations, based on the low and high-frequency fluctuations of measured rotor thrust and torque, is used to assess the impact of the flaps on the blade cumulative damage and the fatigue lifetime for both upwind and downwind configurations. From a practical standpoint, strategies of using flaps to mitigate blade cumulative damage as well as improve turbine power and yaw stability for both upwind and downwind configurations are recommended as follows:

➢ Upwind configuration:

- Flaps with an angle of 30° decrease the blade cumulative fatigue damage for all yaw angles and reduced the rotor torque unsteady loads for yaw angles of +8° and ±16° where there is no adverse effect on the wind turbine yaw stability. Therefore, it is recommended to use the flaps with an angle of 30° for yaw angles of +8° and ±16° while a marginal power reduction should be considered. It is worth noting that in the case of zero and -8° yaw angles, flaps with an angle of 30° decreases the blade cumulative fatigue damage while increasing the rotor torque unsteady loads with a marginal reduction in turbine power. Therefore, it is not recommended to use flaps in the case of zero and -8° yaw angles and the control system can command to close the flaps (in the case of an adjustable flaps system).

➢ Downwind configuration:

- It is highly recommended to use the flaps with an angle of 60° for yaw angles of 0°, ±8°, and +16° and the flaps with an angle of 30° for a yaw angle of -16° for downwind configuration considering the maximum reduction in the blade cumulative fatigue damage and the maximum improvement in the ratio of turbine power and turbine thrust (C_P/C_T) as the criteria for the recommended flap.

- It is worth noting that using flaps in downwind configuration compensates for the adverse effect of wind turbine yaw misalignment on the wind turbine performance and unsteady loads.

- Using flaps decreases the cut-in speed and therefore increases the turbine annual energy yield by increasing wind turbine power generation for downwind configuration.

- The simulations show that the activation of the flaps amplifies the wind turbine's power output. Additionally, the yaw stability is increased. But these effects are accompanied by an increased thrust. The trends in the 'quasi-steady' variance of the rotor torque can be stated: The rotor torque's variance decreases with increasing flap angle. The torque at the tower wake passage is increased by the flaps. The simulations also predicted increased yaw stability and a decrease in the rotor torque's variance, which are both desirable effects. The simulation results are in good agreement with the experiments.

Theoretical explanations indicate that in the case of upwind configuration, increasing downstream velocity (slowing down upstream velocity) leads to a marginally decrease in turbine power (turbine Euler equation) and consequently may marginally increase the torque amplitude ratio. However, lower wind speeds seen by inner spans lead to mitigate thrust load generated by inner spans. In the case of downwind configuration, increasing upstream velocity leads to improve turbine power based on the turbine Euler equation, and pushing flow to outer spans with higher lift/drag ratios leads to mitigate unsteady loads (thrust and torque) generated by inner spans.

It is worth noting that in using flaps as a passive approach to mitigate unsteady loads, four points should be considered: Firstly, using flaps increases the weight of nacelle and may need modifications in nacelle design in order to install flaps as well as actuators and hydraulic system. Therefore, it is needed to double-check the structural loads. Secondly, adding flaps and a control system to adjust the flaps during wind turbine operation increases the initial investment cost and it should be taken into account by manufacturers in order to make flaps more economically viable in future designs. Thirdly, a lower overload factor may decrease the risk of pitting and bending damage in gearboxes, and also may decrease lubricant temperature in bearings and gearbox due to lower local contact pressure. Thus, the operational and design conditions of bearings and gearbox should be considered especially where there is an increase in the maximum of the turbine power (torque) during a rotor revolution by using flaps. Finally, as the control system of multi-megawatt wind turbines generally works based on controlling the rotor speed by adjusting the rotor torque using a collective blade pitch control, the control logic should be updated especially when there is an increase in rotor torque by using flaps.

6 Future Activities

At the outset of this project ETH had Hitachi Ltd. of Japan as the industrial partner, with the expectation that the industrial partner could be involved in feasibility studies and cost modeling. However, in January 2019 Hitachi decided to stop their development and manufacturing of downwind turbines. Thus, Hitachi could not disclose to ETH relevant costs that could have been used for cost modelling. Therefore, while based on technical performance we have made recommendations to national and international bodies regarding nacelle modifications, that is flap settings, for upwind and downwind wind turbine configurations, in future work, if relevant cost data we available, it would be useful to conduct cost modeling studies.

7 National and International Cooperation

Through the Hitachi-funded project at ETH “Load Alleviation and Control of Floating Multi-Megawatt Downwind Turbines,” this project leveraged the strong industrial partnership that ETH had with Hitachi Ltd. of Japan. ETH served as the primary university technology development partner of Hitachi, Ltd. As Hitachi, Ltd. is based in Japan that has complex terrain quite similar to the terrain of Switzerland, and Hitachi, Ltd. was the world’s leading commercial manufacturer of downwind turbines [16] this strong link to Hitachi Ltd. enhanced this project. ETH communicated outcomes from both this project, as well as the Hitachi funded project at meetings of IEA Wind Task 40 “Downwind Turbines”. Sadly, in January 2019 Hitachi decided to stop their development and manufacturing of downwind turbines, although the Hitachi-funded project at ETH remained funded. The end of Hitachi’s wind turbine development constrained ETH’s dissemination activities.

8 Communication

The present work was also linked to the IEA Wind Task 40 “Downwind Turbines”. In Task 40, ETH led a work package related to quantifying the impact of the nacelle on turbine operation. The outcomes of the experiments were used to support the development of an engineering model that can be integrated into a design tool.

A Ph.D. student and a mechanical engineering Master’s student were involved in this project.

9 Publications

- H Hoghooghi, S Blaser, N Chokani, R S Abhari, “Alleviation of Unsteady Loads on Wind Turbines Using Optimised Nacelles,” draft manuscript for journal in preparation, 2020.
- S Blaser, “Nacelle Optimization for Improved Wind Turbine Performance,” Masters Thesis, Laboratory for Energy Conversion, ETH Zürich.

10 Bibliography

[1] Swiss Federal Office of Energy SFOE, “Energiestrategie 2050: Stand nach der Zweitberatung im Nationalrat” (German only), Mar. 2016.

[2] Swiss Federal Office of Energy SFOE, “Schweizerische Elektrizitaetsstatistik 2014” (German only), Jul. 2015.

[3] Swiss Federal Office of Energy SFOE, “Energieperspektiven 2050” (German only), Oct. 2013.

[4] European Commission, “A Policy Framework for Climate and Energy in the Period from 2020 to 2030”, Jan. 2014.

[5] Frau E., Kress C., Chokani N., Abhari R.S., “Comparison of performance and unsteady loads of multimegawatt downwind and upwind turbines,” ASME Journal of Solar Energy Engineering, 137, 041004, 2015.

[6] Kress C., Downwind wind turbine performance, loading and design considerations, Ph.D. thesis, ETH Zurich, No. 23329, 2016.

[7] White F M. Fluid Mechanics, 7th ed., New York, McGraw-Hill, 2009.

[8] Sutherland H J. Summary of the Fatigue Properties Wind Turbine Materials. Sandia National Laboratories, Wind Energy Technology Department, 2000, Albuquerque, New Mexico, 199, 87185-0708.

[9] da Rocha Teixeira R E. Fatigue Analysis of Wind Turbine Blades. Master thesis, Mechanical Engineering Department, Faculty of Engineering of the University of Porto, 2014.

[10] Mandell J F, Reed R M. Samborsky D D. Fatigue of Fiberglass Wind Turbine Blade Materials. Department of Chemical Engineering Montana State University, 1992.

[11] Sutherland H J, Mandell J F. Application of the U.S. high cycle fatigue database to wind turbine blade lifetime predictions. Proceeding of Energy Week, ASME, 1996.

[12] Miner M A. Cumulative damage in fatigue. Journal of Applied Mechanics, 1945, 12, A159–A164.

[13] Grewal S. Gas turbine engine performance deterioration modeling and analysis. Ph.D. thesis. Cranfield Institute of Technology, England, 1988.

[14] Panagiotis N. Airfleet maintenance case study. Bachelor's thesis. University of Western Macedonia, Greece, 2015.

[15] IEC-61400. International Electrotechnical Commission, IEC, 2012.

[16] Saeki M., Tobinaga I., Sugino J., Shiraishi T. Development of 5-MW offshore wind turbine and 2-MW floating offshore wind turbine technology. Hitachi Review, 63(7) 414-421, 2014.